Stability, transition and turbulence in rotating cavities

Chapter · January 2004

DOI: 10.2495/1-85312-785-X/05

4 authors:

Emilia Crespo del Arco
National Distance Education University
62 PUBLICATIONS **608** CITATIONS
SEE PROFILE

Eric Serre
Aix-Marseille Université
337 PUBLICATIONS **3,825** CITATIONS
SEE PROFILE

P. Bontoux
Aix-Marseille Université
278 PUBLICATIONS **2,278** CITATIONS
SEE PROFILE

Brian Launder
The University of Manchester
427 PUBLICATIONS **53,777** CITATIONS
SEE PROFILE

E. Crespo del Arco, E. Serre, P. Bontoux, BE Launder,
"Stability, transition and turbulence in rotating cavities"
in INSTABILITY OF FLOWS (ISBN: 1-85312-785-X, ISSN 1353-808X)
Edited by M. Rahman. 141-195, WIT PRESS 2005

Stability, transition and turbulence in rotating cavities

E. Crespo del Arco[1], E. Serre[2], P. Bontoux[2] & B.E. Launder[3]

[1]*Dpto Física Fundamental, UNED, Apdo. 60.141, 28080 Madrid, SPAIN*

[2]*Laboratoire de Modélisation et Simulation Numérique em Mécanique et Génie des Procédés, UMR 6181 CNRS/Univ. Aix-Marseille, IMT, La Jetée, 38 rue Joliot-Curie, 13451 Marseille, FRANCE*

[3]*Dpt. of Mechanical, Aerospace and Manufacturing Engineering, UMIST, Manchester M60 1QD, UK*

Abstract

This chapter reviews striking features of boundary-layer instabilities induced by different mechanisms and related to transition to turbulence in rotating flows with walls. Besides its fundamental importance as a three-dimensional prototype flow, confined flow between rotating discs has been extensively examined because of its relevance to many industrial applications such as turbomachinery and engineering processes. Many studies using stability analyses and experiments have been devoted to the onset of unstable waves and to the mechanisms associated with them. Here, we focus on how numerical investigations may provide insights and complement experimental data and analytical results by providing the full velocity field in well-controlled flows within idealized configurations. Rotor-stator and rotating cavity with radial throughflow are investigated. At a critical rotation rate, axisymmetric and/or three-dimensional structures appear in the Bödewadt and Ekman layers. All features of the transitions in these rotating cavities are documented. A comparison of the wave numbers, frequencies, and phase velocities of the instabilities with available theoretical and experimental results shows that both Type II (or A) and Type I (or B) instabilities appear, depending on flow and geometric control parameters. Interesting patterns exhibiting the coexistence of circular and spiral waves are found under certain conditions.

1 Introduction

Flows in rotating-disks systems are not only a subject of fundamental interest as prototype flows for three-dimensional boundary layers but are also a topic of practical importance in the performance improvement of many industrial devices. In turbomachinery, typical flow configurations are flows between rotating compressor and turbine disks, which can be idealized as flows confined between two coaxial rotating disks. Rotor-stator flows and forced source-sink flows with rotating walls are the main configurations investigated theoretically, numerically and experimentally (Section 5). Many of these flows also have features that appear in the flow in the earth's atmosphere and in wind-driven surface layers of the ocean and thus have applications to geophysics too. In these two-disk flows, boundary layers develop at high rotation rates caused by a differential rotation rate between solid boundaries and the incompressible fluid in rigid-body rotation in the core of the cavity (Section 4). The transition process to turbulence is governed by instabilities that arise within these boundary layers. The identification and characterization of mechanisms related to this process should improve prediction methods and lead to new, more efficient control strategies both of considerable importance in practical flows. Despite intensive work and recent advances, no full understanding of the transition and the turbulent breakdown process has yet been achieved in these flows. A review of recent advances in the study of rotor-stator and source-sink flows transition processes are given in Sections 7 and 8.

Bödewadt, Ekman and von Kármán boundary layers are particular cases of this family of rotating boundary-layer flows that are exact solutions of the Navier-Stokes equations (Section 3). Consequently, they have been extensively studied since the Ph. D. Thesis of Ekman 1902, which was a theoretical study of the influence of the Earth's rotation on wind-driven ocean currents. The Ekman layer is produced when the wall and the fluid at infinity approach the same rotation rate. In 1940, Bödewadt studied the flow produced near a stationary disk in fluid rotating at infinity with uniform angular velocity. In the von Kármán boundary layer, the flow is produced by an infinite disk rotating in still fluid.

From linear theory going back to Lilly [1] it is known that the Ekman flow may become unstable to two different instabilities, designated Types I and II. The Type I is related to an inflection point in the velocity profile, similar to the Tollmien Schlichting instability of the boundary layer on a flat plate, while the Type II is viscous. Since then, numerous works have been devoted to the investigation of these instabilities that appear also in Bödewadt and von Kármán boundary layers. Basically, in linear stability analysis, one considers a basic perturbation in the form of a plane wave, which in one dimension is $\exp\left(ikr + i\beta\theta - i\sigma t\right)$ with k, β, σ satisfying the dispersion relationship $D\left(\sigma, k, \beta\right) = 0$. In many problems one must take k to be real and distinguish between stable $\left(Im\left(\sigma\left(k\right)\right) \leq 0\right)$ and unstable disturbances $\left(Im\left(\sigma(k)\right) > 0\right)$ for a particular k value. More recent insight on the transition process in these boundary layers has been gained by considering the response to a brief and localized perturbation introduced into the unstable boundary layer region. Indeed, in some cases it may be insufficient to treat the time

development of a system by considering just a single mode with a specific wave number k, as is treated in linear stability analysis (temporal framework). It may be necessary to consider a spatial pulse or wave packet composed of a range of k values and study the evolution with time at every location in space (spatial framework). When an impulse response grows with time at every location in space, the flow is defined as *absolutely unstable*. By contrast, when the response propagates away from any point sufficiently rapidly and the disturbance decays at every location in a sufficiently long time, the flow is defined as *convectively unstable*. Interest in the rotating-disk flows has been renewed by the study of Lingwood [2, 3, 4] on the convective and absolute character of the instabilities in these flows. In Table 1, critical Reynolds numbers, based on the local radius, obtained from stability analysis using temporal and spatial frameworks are given for the three types of rotating boundary layers.

Table 1: Critical Reynolds numbers obtained in the stability analysis using temporal and spatial frameworks for the three basic types of rotating boundary layer flows by Faller [5] and Lingwood [3]. Ro is the Rossby number further defined in eqn. (1).

Rossby number	Type II	Type I	Neutral stability for stationary waves $\sigma = 0$	Absolute instability
$Ro = -1$ (Kármán)	69.4	285.3	290	507
$Ro = 0$ (Ekman)	54.3	113.1	116.3	198
$Ro = +1$ (Bödewadt)	15.1	$[15.1; 25]$	27.4	21.6
	Temporal framework k real, σ complex [5]		Spatial framework k complex, σ real [3]	

The effect of spatial inhomogeneity on the global response of the locally absolutely unstable flow is the subject of very recent studies (see [6, 7]). A major finding in the understanding of the turbulent breakdown process is that the onset of absolute instability in both the von Kármán and Ekman layers was found to occur at a value of Reynolds number that closely corresponded to the value obtained experimentally for the laminar-turbulent transition. Further insight on this point was recently given by Pier [8].

Investigation of turbulent flows in rotating-disk systems is naturally of great practical importance (Section 9). Moreover, the disk boundary layer provides a

most canonical platform for investigating the underlying structure of the three-dimensional boundary layer. Fundamental studies have shown that rotation substantially affects turbulence, for example by reducing the dissipation rate [9], increasing the anisotropy [9] and greatly reducing the extent of the logarithmic wall region (or, indeed, of eliminating it altogether) [10]. This underlines that, to achieve a reasonable width of applicability within the framework of Reynolds averaging, one needs to shift attention from isotropic effective viscosity approaches to representing the mixing processes. Indeed, as we note in Section 9, it seems that the impact of large-scale, organized structures, which are known to form in disk cavities under certain conditions, will only be resolvable numerically with a time-dependent treatment. The simplest useful level of such treatment is as we discuss still the subject of research enquiry.

Major research efforts in numerical fluid mechanics have also to take into account new knowledge on the physics of turbulence and its use in turbulence modelling. The solution of engineering problems requires improved turbulence models in order to ensure that they can be solved by using the time-averaged form of the Navier-Stokes equations, the so-called Reynolds equations. Hence, research groups on physics of turbulence and turbulence modelling in rotating flows have to be established that go beyond the knowledge that was derived on turbulence in the first half of the 20th century. To stay with the existing models of turbulence, i.e. using isotropy assumptions, will be insufficient for future numerical work to solve rotating fluid-flow problems in which the turbulence is strongly inhomogeneous and anisotropic. In the Appendix of this chapter, general features about numerical approaches used today to solve fluid mechanics equations are presented. Following great advances in numerical methods and computer power, numerical approaches have today become very effective at describing and analyzing accurately flows during the laminar-turbulent transition process. High-performance computer developments have provided an increase in computational speed by roughly a factor 10 every 5 years. In the last three decades, a factor of 10 every 8 years was also achieved by advanced numerical techniques (Figure 1). All these developments together now permit numerical solutions of three-dimensional time-dependent complex phenomena at high Reynolds numbers.

2 The Reynolds and Rossby numbers

The nonlinearity of the Navier-Stokes equations makes it important to evaluate the magnitude of the different terms to make further simplification. The characteristic scales of the flow are thus introduced: L is a typical length scale, U the velocity, Ω the angular velocity and ν the kinematic viscosity of the fluid. Two dimensionless numbers may then be derived from these scales.

The Reynolds number characterizes the relative importance of the momentum transport in the fluid by advection and viscous diffusion and it is defined as

$$Re = \left| \frac{\mathbf{v} \cdot \nabla \mathbf{v}}{\nu \Delta \mathbf{v}} \right| = \frac{UL}{\nu}.$$

The Rossby number which compares the advection and the Coriolis effects, is defined as

$$Ro = \left| \frac{\mathbf{v} \cdot \nabla \mathbf{v}}{2\Omega \times \mathbf{v}} \right| = \frac{U}{L\Omega}.$$

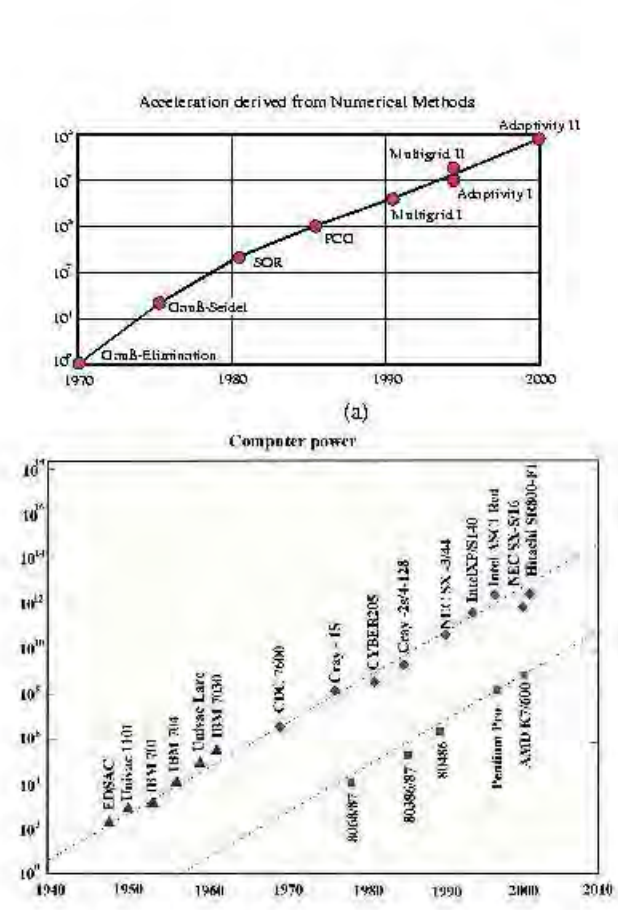

Figure 1: Speed up of numerical computations due to numerical methods (a) and increase in computer power (b).

Coriolis force dominates if $Ro << 1$. If the Reynolds number $Re >> 1$ and the Rossby number is small, a first approximation to the momentum equation for incompressible flows is to balance the Coriolis force with the radial pressure gradient. This approximation is used for almost inviscid, nearly steady flows of small amplitude.

In the literature concerning rotating boundary layers a range of different reference magnitudes for U and L are used. In many cases the reason is that U is not known *a priori* but is a result experimentally or theoretically obtained. Thus, the unit speed U depends on the specific problem. A characteristic length applicable in many cases, is given by $\delta = (\nu/\Omega)^{1/2}$, the characteristic depth of the rotating boundary layer.

In the flow over a rotating disk the relevant Reynolds number proposed by Faller [5] is the boundary layer Reynolds number Re_δ, which is written:

$$Re_\delta = \frac{(\Omega_f - \Omega_d) r^* \delta}{\nu} = \frac{r^*}{\delta} Ro,$$

where Ro, a Rossby number, is

$$Ro = \frac{\Omega_f - \Omega_d}{\Omega}, \tag{1}$$

$$\text{with } \Omega = (\Omega_f + \Omega_d)/4 + \left((\Omega_f + \Omega_d)^2/16 + (\Omega_f - \Omega_d)^2/2 \right)^{1/2},$$

and Ω_f and Ω_d are the fluid angular velocity outside the boundary layer (i.e. in the core) and the disk angular velocity.

In the case of the flow between two disks, the reference velocity can be chosen as $\Omega_d H$, where H is the height of the cavity, and the Reynolds number is $Re = \Omega_d H^2/\nu$. Large values of Re are typical of the case where the boundary layers on the two disks are separate, while small Re are characteristic of the merged boundary layers (see Greenspan [11] and Section 4 for further details). In finite disk systems, the Reynolds number can also be based on the external radius of the cavity, $Re_R = \Omega_d R_1^2/\nu$.

In the following, we will use Re as the general physical parameter but we will also incorporate Re_δ in the discussion of stability thresholds and characteristic wave parameters.

3 Flow near a rotating disk

Consider the flow induced in a homogeneous fluid rotating at an angular rate Ω_f by a disk rotating at angular speed Ω_d about the same axis of rotation. The radius of the disk and the extent of the fluid above the disk are taken to be infinite. Differential rotation between the disk and the incompressible fluid in relative rotation causes boundary layers flows. Depending upon the relative values of Ω_f and Ω_d

three types of rotating boundary-layer-flows can be defined (see [12, 13]). The von Kármán boundary-layer flow arises when the fluid at infinity is at rest, $\Omega_f = 0$, and the disk rotates with $\Omega_d = \Omega$, then $Ro = -1$. In the Bödewadt layer flow the disk is at rest, $\Omega_d = 0$, and the fluid rotates at $\Omega_f = \Omega$ ($Ro = 1$). In the Ekman layer flow the fluid at infinity and the disk approach the same rotate $\Omega_f \approx \Omega_d = \Omega$ ($Ro = 0$). Both the linear Ekman layer and the von Kármán flow are exact solutions of the Navier-Stokes equations and have constant boundary layer thickness. But while the von Kármán boundary layer has a Reynolds number that varies with radius (due to the radius dependence of the characteristic velocities), the Ekman layer can have constant geostrophic velocity giving a single Reynolds number definition of the flow.

In the Ekman and von Kármán boundary-layer flows, the fluid is thrown radially outwards due to the action of centrifugal forces and is replaced by downwards axial flow (Figure 2). On the other hand, in the Bödewadt flow, there is an equilibrium of centrifugal forces and radial pressure gradient forces in the fluid rotating at infinite distance above the disk but the centrifugal force is reduced within the boundary layer, due to viscous action, and the axially independent radial pressure gradient causes a radial flow that is predominantly inwards (Figure 3).

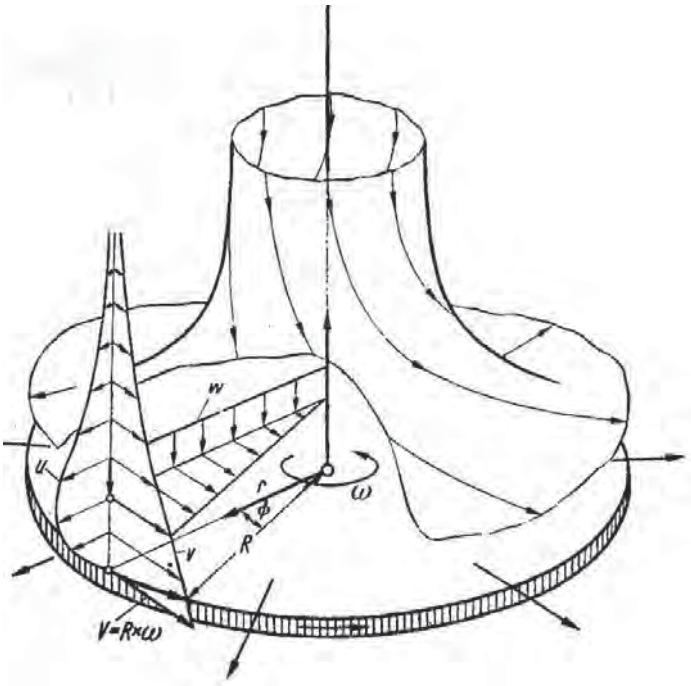

Figure 2: Rotation of the disk in a still fluid (von Kármán layer). Velocity components : u-radial, v-tangential, w-axial. Owing to the centrifugal force, the secondary flow is directed radially outwards (from Schlichting [12]).

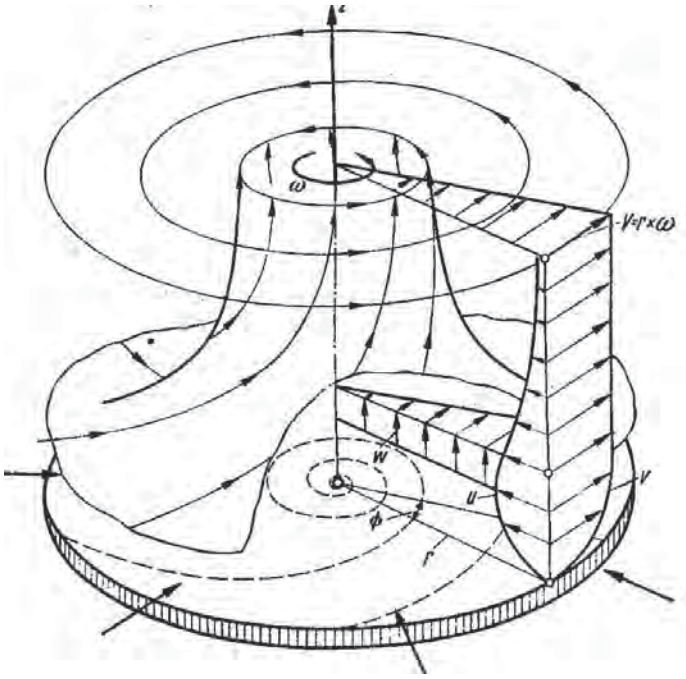

Figure 3: Rotation of flow near a stationary disk (Bödewadt layer). Velocity components : u-radial, v-tangential, w-axial. Owing to friction, the secondary flow is directed radially inwards (from Schlichting [12]).

These boundary-layer flows become unstable when Re_δ exceeds a critical value. Two basic types of linear instability for corotation of the fluid and the disk have been documented both experimentally and theoretically. Historically these are referred to as Type I (or Type B) and Type II (or Type A) instabilities and both instability types have been observed when the disk is differentially rotating slower or faster than the fluid. The Type I instability is due to the presence of unstable inflection points in the boundary-layer velocity profile. It is also referred to as a "crossflow" instability, observed in the flow over a swept wing, where it consists of a series of standing vortices in the boundary layer (see Ref. [14]). The linear stability analysis of Lilly [1] of the Ekman-layer flow showed that the Type II instability has a lower critical Reynolds number than the Type I. The mechanism for Type II instability is related to the combined effects of Coriolis and viscous forces. Both instabilities are found theoretically and experimentally in the three types of boundary layers with nevertheless large differences in the critical Reynolds number for the onset (see Refs. [4, 5]). Some characteristic parameters from theoretical and experimental results are reported in Tables 2-4 for the Ekman, Kármán and Bödewadt layers, respectively.

The disturbed flow due to instabilities may sometimes be referred to as waves

and sometimes as vortices. The disturbances have vorticity, and when the basic flow is subtracted from the total flow they appear as vortices. But, in terms of the total flow, the instability appears as a waviness of the streamlines as illustrated by the photograph (Figure 4) from the experiment of Faller and Kaylor [15].

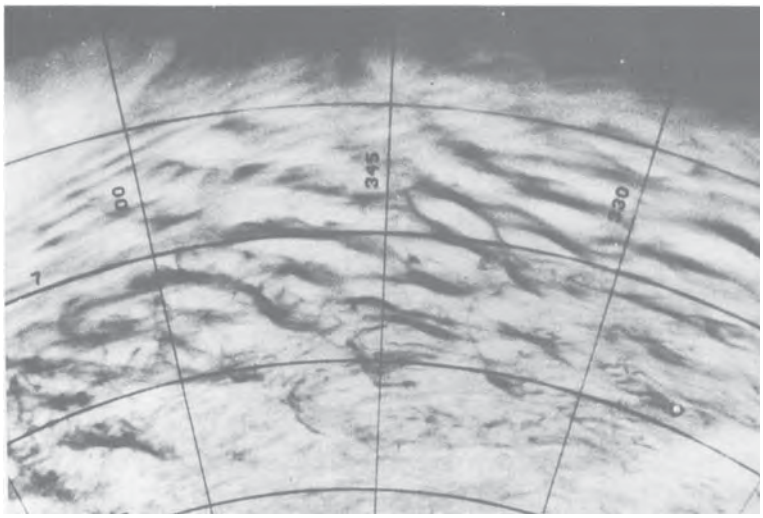

Figure 4: Flow visualization of waves related to Ekman-layer instability (from Faller and Kaylor [16]).

The analysis differentiating between convective and absolute instabilities is based on linear theory. The methods of distinguishing between them have been developing over the past thirty years. The most rigorous and general method was given by Briggs [17]. For all the flows an absolute instability is caused by a pinch point between a spatially growing and a spatially damped branch of the dispersion relation. For details see the excellent review on absolute and convective instability and its relationship with global instability by Huerre and Monkewitz [18] for the case of shear flows and by Huerre [19] for the case of flow over a rotating disk. In the study of rotating-disk boundary layers, the most important recent developments on the convective and absolute character of the instability are certainly due to Lingwood [2, 3, 4] (see also additional references in [6, 7]). Lingwood [4] studied the onset of absolute instability for Ro in the interval $[-1, 1]$ (Figure 6). Lingwood [4] showed that as Ro tends to 1, the flows become increasingly unstable in both the convective and absolute senses. In the limit ($Ro = 1$), for the Bödewadt layer the onset of convective and absolute instability occurs almost simultaneously at very low Re (Figure 6). Lingwood [2, 3] exhibited theoretically and experimentally a transition from local linear convective to absolute instability at a radius that closely corresponds to the onset location of experimentally observed turbulence. More recently Pier [8] showed that transition to turbulent flow coincides with a

secondary absolute instability of the naturally selected primary nonlinear crossflow vortices that prevail for a wide range of azimuthal wave numbers as shown in Figure 5. A secondary disturbance growing in time at fixed radial locations continuously perturbs the primary vortices, thus triggering the direct route to turbulence prevailing in this configuration. The state of this problem has recently been reviewed by Reed and Saric [7].

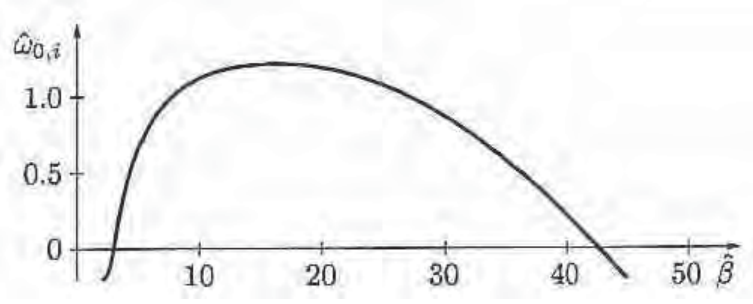

Figure 5: Secondary absolute growth rate $\omega_{0,i}(\widehat{\beta})$ pertaining to primary crossflow vortices near the onset of nonlinearity. Because of the shape of the curve, Pier named this the "elephant" mode (From Pier [8]).

3.1 The Ekman layer

In geophysical flows the Ekman layer is found when there is a geostrophic flow (i.e. there is a balance between Coriolis and horizontal pressure gradient force) near a surface or boundary. For instance, steady winds blowing over the sea surface produce a thin horizontal Ekman boundary layer, a few hundred meters thick. A similar boundary layer exists at the bottom of the ocean, the bottom Ekman layer, and at the bottom of the atmosphere just above the sea surface, the planetary boundary layer. The planetary boundary layer is the part of the atmosphere strongly influenced by the presence of the earth surface.

The first significant advance in the study of wind-driven currents was made by Fridtjof Nansen and Vagn Walfrid Ekman. In 1893 Nansen, who was a biologist, led an expedition towards the North Pole. After two years adrift he concluded that the ship did not drift downwind. Instead, he observed that wind tended to drive ice at an angle 20^o to 40^o to the right of the wind. In the explanation given by Nansen, which is correct, the main argument was that the motion of the ice is the result of three forces: wind stress, friction or drag when the ice moves in the water, and Coriolis force [20]. The forces must have the following attributes:

- Drag must be opposite to the direction of the ice's velocity
- Coriolis force must be perpendicular to the velocity
- The forces must balance for steady flow.

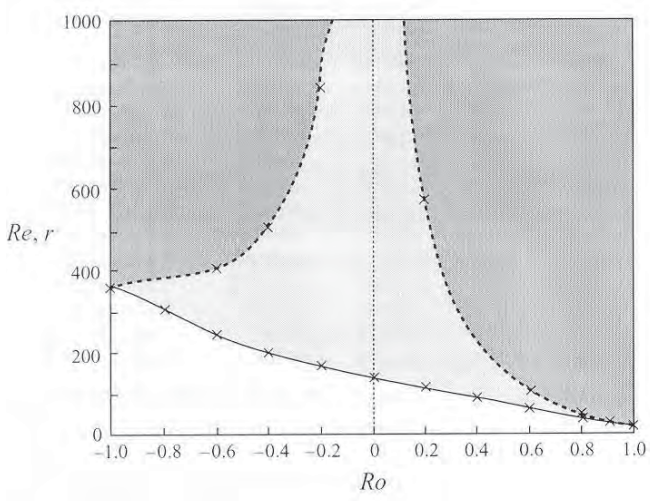

Figure 6: Critical Reynolds number (line) and radii (dashed line) for the onset of absolute instability for the Bödewadt-Ekman-Kármán system. The bounding lines are fitted to the calculated data points (cross) and the shaded areas correspond to the absolutely unstable regions (from Lingwood [4])

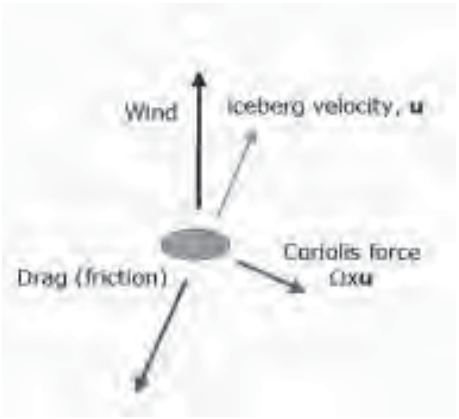

Figure 7: Scheme of the different acting forces illustrating the quantitative arguments of Nansen to predict the ice motion.

The theoretical study of the influence of Earth's rotation on wind-driven ocean currents was the subject of the Ph. D. Thesis of Ekman in 1902, under the tutelage of Vilhelm Bjerkness and Fridtjof Nansen. Ekman assumed a steady, homogeneous horizontal flow with friction on a rotating Earth and obtained the solution known

as an Ekman spiral. Since in nature, both in the atmosphere and in the ocean, the boundary-layer flows are usually turbulent, Ekman obtained a solution for the mean flow assuming that the Reynolds stresses could be modelled via an eddy viscosity. However, the analytical solution of Ekman is strictly applicable to laminar flow by replacing eddy viscosity with a constant dynamic viscosity in the time-averaged Navier-Stokes equations. As illustrated in Figure 8, in the northern hemisphere the Ekman layer, the current on the sea's surface will point 45 degrees to the right of the wind's direction, and as you go deeper, the current speed decreases while turning in a clockwise direction.

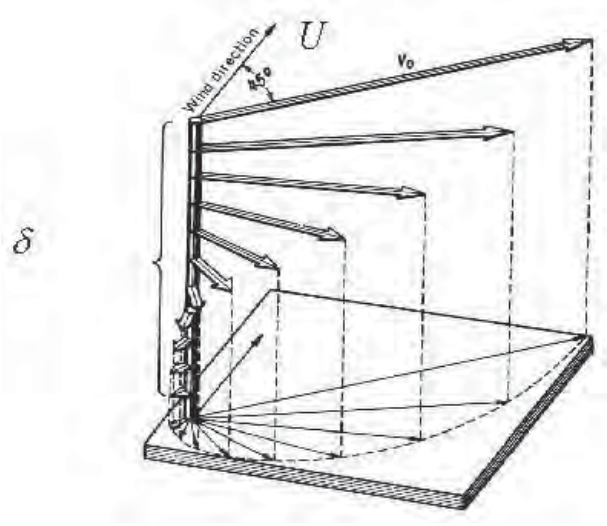

Figure 8: Schematic illustration of the vertical distribution of currents due to wind blowing on the sea surface.

The solution of the Ekman boundary layer flow can be obtained analytically (see for instance Ref. [21] for a turbulent flow and Ref. [22] for a laminar flow) and if u^*, v^* are the velocity components in the (x, y) plane, parallel and perpendicular to the geostrophic velocity respectively the solution for flow over a rigid surface at $z^* = 0$ is,

$$\begin{aligned} u^* &= V_\infty^* e^{-z^*/\delta} \sin z^*/\delta, \\ v^* &= V_\infty^* \left(1 - e^{-z^*/\delta} \cos z^*/\delta\right), \end{aligned} \tag{2}$$

where V_∞^* is the velocity of the flow at large distance from the surface and $\delta = \sqrt{\nu/\Omega}$, the reference length of the depth of the Ekman layer. The Reynolds number characterizing this boundary layer flow may be defined using δ and V_∞^*,

$$Re_\delta = \frac{V_\infty^* \delta}{\nu}.$$

Some values of characteristic parameters of Type I and Type II instabilities of the Ekman layer flow are summarized in Table 2.

Table 2: Characteristic parameters of the patterns related to Type I and Type II instabilities in the Ekman boundary-layer flow. Linear stability and experimental results.

References	$Re_{\delta c}$	λ/δ	ε
Linear stability analysis			
Lilly [1]	$Re_{\delta cI} = 110$	11.9	7.5°
	$Re_{\delta cII} = 55$	21	-20°
Faller and Kaylor [15]	$Re_{\delta cI} = 118$	11	10° to12°
	$Re_{\delta cII} = 55$	24	-15°
Faller [5]	$Re_{\delta cI} = 113.1$	11.5	6.9°
	$Re_{\delta cII} = 54.3$	20.1	-23.1°
Itoh [23]	$Re_{\delta cI} = 113$	11.5	7.2°
	$Re_{\delta cII} = 54.2$	21.65	-23.3°
Lingwood [4]	$Re_{\delta cI} = 116.3$	11.5	14.5°
Serre *et al.* [24]	$Re_{\delta cI} = 112.8$	11.49	7.2°
	$Re_{\delta cII} = 54.18$	21.64	-23.3°
Experiments			
Faller [25]	$Re_{\delta cI} = 125$	$[9.6; 12.7]$	$[10^\circ; 16.3^\circ]$
Tatro and	$Re_{\delta cI} = 124.5$	11.8	14.6°
Mollo-Christensen [26]	$Re_{\delta cII} = 56.3$	$[25; 33]$	$[-8^\circ; 0^\circ]$

The critical Reynolds number of Type I instability is about $Re_{\delta cI} \approx 120$. Corotating vortices form, spiralling outward with their axes along logarithmic spirals of angle $90^\circ + \varepsilon$ with respect to the radius of the disk [7]. Typically ε is from 11° to 14.5°. The pattern of Type I instability is almost stationary with $n = 20$ to 30 spiral arms of wavelength of about $\lambda/\delta = 11.5$. Type II instability has a much lower critical Reynolds number, typically $Re_{\delta cII} \approx 55$. In contrast to the Type I instability, the vortex spiral involves a negative or zero ε angle ($-20^\circ \leq \varepsilon_{II} \leq 0^\circ$), and has a larger wavelength than Type I typically in the range $20 \leq \lambda_{II}/\delta \leq 30$. But, although Type II travelling waves have significantly lower critical Re than stationary waves, the Type I instability is more commonly observed in experiments. Thus, in the Ekman-layer experiments, Type II instability only appears when there are

mechanical disturbances ([5, 26, 27]). Nevertheless, all linearized stability analyses reveal that the instability arises as a Hopf supercritical bifurcation.

This apparent discrepancy between experimental and theoretical results has been clarified by the investigation of the absolute or convective nature of the rotating boundary-layer flow (Lingwood [2, 3, 4]). The motivation is that in some systems the determination of the critical conditions for the onset of instability of a single wave number wave is not sufficient and the study of the evolution of a packet wave must be undertaken. The instability may then be classified as convective, in which case the pulse would propagate away from any point, sufficiently rapidly that the disturbance at that point would decay in time. Alternatively, it may be non-convective or absolute, in which case the pulse may still propagate but the disturbance at any point in space would eventually grow with time.

The onset of convective instability of stationary waves agrees quite well with the experimentally observed Reynolds number of about $Re_\delta = 125$. Absolute instability is predicted for $Re_\delta \approx 198$ in the Ekman-layer flow by Lingwood [4]. There is some experimental evidence that the onset of laminar-turbulent transition in the Ekman layer occurs at $Re = 180 - 200$ ([25, 26, 28]) which is consistent with the onset of absolute instability found by Lingwood [4].

Recently, the spatio-temporal evolution of the weakly nonlinear oceanic Ekman-layer model has been studied using perturbation theory. In the infinite-depth case the amplitude equation describing the pattern formation is a Ginzburg-Landau equation since in the finite-depth case the resulting equations are the Davey-Hocking-Stewartson equations [29].

3.2 The von Kármán layer

The steady solution of von Kármán boundary-layer flow is an exact solution of the Navier-Stokes equations in which the nonlinear terms related to the convective acceleration are retained.

The transition of this boundary-layer flow to turbulent has been the subject of much theoretical and experimental work because of the similarity with the transition that occurs in the leading-edge region of a swept wing. In both systems the stationary flows show inflectional cross-flow velocity profiles and the so-called cross-flow instability is possible. This form of instability was first noticed on a rotating disk by Gregory *et al.* [31]. The results of the linear stability of the basic flow to travelling waves are reviewed in Ref. [5].

The patterns associated with Type I and Type II instabilities have almost the same characteristics as in the Ekman-layer flow (Table 3). The critical Re_δ of Type I ($259 \lesssim Re_{\delta cI} \lesssim 300$) is about twice that of the critical Re_δ for the same instability in the Ekman flow while the critical Reynolds number of Type II instability is just slightly larger ($59 \lesssim Re_{\delta cII} \lesssim 69$). The critical wave number lies in the range $22 \leq n \leq 32$. Some effects due to the experiment's finite geometry on the critical wave number selection are discussed in Jarre *et al.* [32].

In the local stability analysis of the von Kármán boundary-layer problem the eigenspectrum has at least three branches. The behavior of Branch 2 at increas-

ingly positive frequency shows that Branch 2 is the Type II instability, described by Faller [5]. Branch 1 is more commonly observed, corresponding to the Type I cross-flow instability. A third mode was discovered by Mack [33] and was also found by Lingwood [2]. There is an absolute instability when Branch 1 and 3 coalesce, giving an absolute instability for $Re_\delta > 507$. Note that when $Ro < 0$, Re_δ is negative but as usually Re_δ will be treated as a positive number. Lingwood showed that for the von Kármán layer, the absolute instability always occur for travelling waves (non-zero frequency) but as the Ro increases towards the Bödewadt layer, the stationary waves can also become absolutely unstable. At lower Re_δ the flow is convectively unstable. The onset of absolute instability is consistent with experimental observations of the critical Reynolds number of laminar-turbulent transition. Comparison between the absolute instability predicted by linear stability analysis and experimental observations for the von Kármán boundary layer is given in Lingwood [2].

The transition value is insensitive to low-level excitation. We note the remark of Huerre [19] that this scenario is different from that prevailing in a non-rotating boundary layer and shear layers where the local transition Reynolds number to turbulence is highly sensitive to the ambient disturbance level and spectral content.

The theoretical analyses of the absolute and convective instability presented before are linear and they are introduced in the framework of the behavior of steady parallel shear flows. The parallel approximation is not verified because the boundary layer on a rotating disk has more depth as the radius increases in the flow direction. The undisturbed velocity also increases with radius, and so the assumption of spatially homogeneous flow is not entirely appropriate. The recent study of Davies and Carpenter [6] investigates how a spatial inhomogeneity affects the global response of this locally absolutely unstable flow.

3.3 The Bödewadt boundary layer

The Bödewadt boundary layer formed on an infinite stationary plane is also an example of a self-similar solution (Bödewadt) but it has received less attention due to the difficulty of reproducing this flow experimentally. In experiments designed to study the Bödewadt layer the fluid and the disk initially rotate and then the disk is suddenly stopped (spin down) [35, 36].

The linear stability results have been summarized by Faller [5]. As with the von Kármán layer, Type I and Type II instabilities may destabilize the flow. However the critical values of Reynolds numbers are very low, with $Re_{\delta cII} = 15.1$, and $Re_{\delta cII} < Re_{\delta cI} < 25$ following the linear analysis of Faller [5]. A recent study of Serre *et al.* [24] confirmed that the Type II instability only exists in a narrow range of Re_δ, disappearing at $Re_\delta = 68$.

The critical value for the onset of absolute instability is predicted by Lingwood [4] at $Re_{\delta c} = 21.6$, and this is very close to the onset of convective instability showing that almost the entire Bödewadt layer is absolutely unstable.

As in the case of the von Kármán solution, the Reynolds number increases radially outwards in the Bödewadt flow. But, as has been remarked by Lingwood [4],

Table 3: Characteristic parameters of the patterns related to Type I and Type II instabilities of the von Kármán layer flow. Linear stability and experimental results.

References	$Re_{\delta c}$	n	ε
Linear stability analysis			
Faller [5]	$Re_{\delta cI} = 285.3$	26	$14.35°$
	$Re_{\delta cII} = 69.4$	6	$-19°$
Pikthov & Smirnov [34]	$Re_{\delta cI} = 285.8$	26	$13.9°$
	$Re_{\delta cII} = 59$	6	$-22.7°$
Lingwood [4]	$Re_{\delta cI} = 290.1$	22	$11.4°$
Experiments			
Wilkinson & Malik [30]	$Re_{\delta cI} = 300$	22	$11° \leq \varepsilon \leq 14°$
Jarre *et al.* [32]	$Re_{\delta cI} = 264 \pm 5$	32	-

since for positive Rossby number convective instability travels outwards toward the absolutely unstable region, in this flow (with negative Rossby number) the convective instability travels inwards towards the stable region where the Reynolds number is lower. Then, as indicated by Lingwood [4] it appears that the behavior of the perturbation is more complicated.

4 Flow between two infinite parallel disks

The flow solutions presented in Section 3 have been extended to the case of flows between two infinite parallel disks by Batchelor [37] who generalized the analyses of von Kármán and Bödewadt to two-parameter families of solutions having a mathematical structure very similar to that of von Kármán's. If the flow solutions above a single disk are described by one parameter (Ro), the flow solutions between infinite disks require two parameters that are the ratio of angular velocities of the disks and the Reynolds number, $Re = \Omega_d H^2/\nu$ based on the gap width between the disks H. Batchelor did not attempt to solve the similarity equations he derived but rather discussed qualitatively their expected features. For the flow between two corotating infinite disks he argued that at high Reynolds number, the fluid between the disk would rotate with a constant angular velocity and that boundary layers would form at both disks. If the boundary layer thicknesses are larger than the gap width H, i.e. if Re is too small, the Batchelor solution evolves to a "torsional Couette-type" flow, the boundary layers being joined.

In this section, we present the particular solution obtained in a rotor-stator configuration and an analytical solution describing the flow between corotating disks with radial outflow obtained from the Ekman solution on a single disk.

Table 4: Characteristic parameters of the patterns related to Type I and Type II instabilities of the Bödewadt layer flow. Linear stability and experimental results.

References	$Re_{\delta c}$	λ/δ	ε
Linear stability analysis			
Faller [5]	$Re_{\delta cII} < Re_{\delta cI} < 25$	-	$-$
	$Re_{\delta cII} = 15.1$	16.6	$-33.2°$
Pikthov and	$Re_{\delta cI} \simeq Re_{\delta cII}$	-	-
Smirnov [34]	$Re_{\delta cII} = 18.8$	-	$-22.4°$
Lingwood [4]	$Re_{\delta cI} = 27.4$	-	-
Serre *et al.* [24]	$Re_{\delta cII} = 18.9$	16.11	$-27.38°$
Experiments			
Savas [35]	$Re_{\delta cII} < Re_{\delta cI}$	$-$	$12° \leq \varepsilon \leq 18°$
	$Re_{\delta cII} = 25$	$11 \leq \lambda/\delta \leq 25$	$0°$

4.1 Flow between a stationary and a rotating disk

In the case of rotor-stator flow, Batchelor [37] showed that three flow regions develop at high rotation rate having the structure of two shear layers near the walls, with a radial outflow close to the rotating disk and a radial inflow close to the stationary disk, bounding an inviscid core rotating at constant angular velocity. The flow is often referred to as "Batchelor flow" in the literature. An alternative similarity solutions was proposed by Stewartson [38] in which a boundary layer would form only at the rotating disk and the core would not rotate. Following the papers of Batchelor and Stewartson there has been a large body of published literature concerning the flow between rotating disks. The review of Zandbergen & Dijkstra [39] provides an extensive survey of theoretical and numerical papers concerning rotating-disk flows. The controversy over the existence of both these solutions was clarified by Mellor *et al.* [40] who numerically demonstrated that both the Batchelor and Stewartson solutions, as well as many others, exist at high Reynolds number for the rotor-stator case.

It is possible to connect the problem of the flow between a rotating and a stationary disk with the single-disk case. Indeed, the solution of Stewartson in the limit of high Reynolds numbers, appears to be the same as the von Kármán solution ($\Omega_f = 0$, $\Omega_d = \Omega$). Moreover, the Batchelor solution can be considered as the connection of two boundary-layer flows at a single disk by an axial flow region in solid body rotation at $\Omega_c = Ro\Omega$, Ro being the Rossby number. At the rotating disk, the boundary layer is defined by $\Omega_f = \Omega_c$ and $\Omega_d = \Omega$ while, at the sta-

tionary disk, the flow is a Bödewadt boundary layer with $\Omega_f = \Omega_c$ and $\Omega_d = 0$. Pearson [41] calculated that $\Omega_c = 0.313\Omega_d$.

The multiplicity of the solutions of the rotating-disk similarity equations, as well as the many physically meaningless velocity fields that are solution branches of the mathematical problem, call into question the ability of the similarity solution to describe the real flow it is intended to represent the flow between rotating finite disks. Brady and Durlofsky [42] investigated the validity of the similarity solution in describing the flow between two finite rotating disks. These authors showed that the presence of an end wall closing the cavity may modify the similarity solution and that its effect increases with increasing Reynolds number. Moreover, these authors showed that the closed-end flows resemble the Batchelor solution while the open-ended flows resemble the Stewartson solution. For $Re \leq 80$, both the open- and closed-end flows agree with the Batchelor solution near the axis of rotation. As the Re is increased the open-flow tends away from the Batchelor toward the Stewartson solution, while the closed-end flow continues to resemble the Batchelor solution. Moreover, in contrast to infinite-disk systems, the base flow in finite-disk systems is unique [43] and is either of Batchelor or Stewartson type depending on the end-wall conditions.

The stability of the Stewartson flow is given by the stability of the von Kármán boundary-layer flow. At large Reynolds number ($Re \simeq 1000$), the linear stability problem of the Batchelor flow is equivalent to the linear stability of both boundary layers separated by a geostrophic core rotating at $\Omega_c = 0.313\Omega_d$ [23]. Indeed, the characteristic parameters of the patterns found in the two-disk problem by Itoh [23] agree very well with the results of Pikhtov and Smirnov [34] obtained in a single rotating disk at Ω_d and a flow rotating at Ω_c. Also, it was determined that the flow may be unstable to Type I and Type II instabilities in both layers, and the first instability of Batchelor flow appears in the Bödewadt boundary layer, at values of the critical Reynolds numbers that are much smaller than in the rotating-disk boundary layer. An important remark is that the local critical Reynolds numbers are independent of Re as soon as Re is large enough ($Re \gtrapprox 500$) so that the core velocity reaches its asymptotic value, $\Omega_c = 0.313\Omega_d$. The characteristic parameters of the patterns related to Type I and Type II instability obtained in the linear stability analysis of a Batchelor flow at $Re = 1000$ are summarized in Table 5.

The linear stability analysis of San'kov and Smirnov [44] for a large range of Reynolds numbers showed that four types of instability, and denoted I to IV, may become unstable depending on the Reynolds number. For Reynolds numbers in the range $112.5 \leq Re \leq 1000$ instabilities denoted III and IV are identified by San'kov and Smirnov with Type I and Type II instabilities of a Batchelor flow with separate boundary layers. At smaller values of Reynolds number ($Re < 112.5$), the base flow is a pure viscous flow with merged boundary layers. San'kov and Smirnov identified two instabilities denoted I ($Re < 21$) and II that are characterised by spiralling vortices with a positive (I) or negative (II) angle and travelling outward (I) or inward (II).

Table 5: Characteristic parameters of the patterns related to Type I and Type II instability obtained in the linear stability analysis of a Batchelor flow at $Re = 1000$. n is the number of spiral arms over 2π.

Stationary-disk boundary layer	$Re_{\delta c}$	n	ε
(Bödewadt layer)			
Itoh [23]	$Re_{\delta cI} = 26.9$	–	$1.6°$
	$Re_{\delta cII} = 21.6$	–	$29.8°$
Serre *et al.* [24]	$Re_{\delta cI} = 35.5$	–	$0.8°$
	$Re_{\delta cII} = 35.5$	–	$-34.6°$
		–	
Rotating-disk boundary layer			
(Kármán boundary layer)			
$\Omega_f \simeq \Omega_d/3$			
Itoh [23]	$Re_{\delta cI} = 281$	22	$10.9°$
	$Re_{\delta cII} = 85.3$	9	$-24.7°$
Serre *et al.* [24]	$Re_{\delta cI} = 278.6$	–	$10.9°$
	$Re_{\delta cII} = 90.23$	–	$-26.3°$

4.2 Flow between two rotating disks

Consider two parallel infinite disks separated by a distance H: one disk is located at $z^* = -H/2$ and the other one is at $z^* = H/2$. Both disks rotate at the same speed Ω involving an axial symmetry of the flow with respect to the plane $z^* = 0$. Then, it is possible to connect the solutions obtained in an Ekman-boundary layer flow on a single disk in eqn. (2):

$$u^* = -V_\infty^* \Big[e^{-(z^*+H/2)/\delta} \sin(z^* + H/2) \, /\delta + e^{(z^*-H/2)/\delta} \sin(z^* - H/2)/\delta \Big] \tag{3}$$

$$v^* = V_\infty^* \Big[1 - e^{-(z^*+H/2)/\delta} \cos(z^* + H/2)/\delta - e^{(z^*-H/2)\delta} \cos(z^* - H/2)/\delta \Big] . \tag{4}$$

It is evident that $u^* = v^* = 0$ at $z^* = \pm H/2$ (no-slip boundary conditions at the disks) and $u^* = 0$, $v^* = V_\infty^*$ at $z^* = 0$. Calculation details can be found in Pedlosky [21].

This analytical solution consists of a uniform geostrophic flow in the axial direction, supplemented by a thin Ekman layer on $z^* = -H/2$ and another Ekman layer on $z^* = +H/2$. A sketch of the solution is shown in Figure 9:

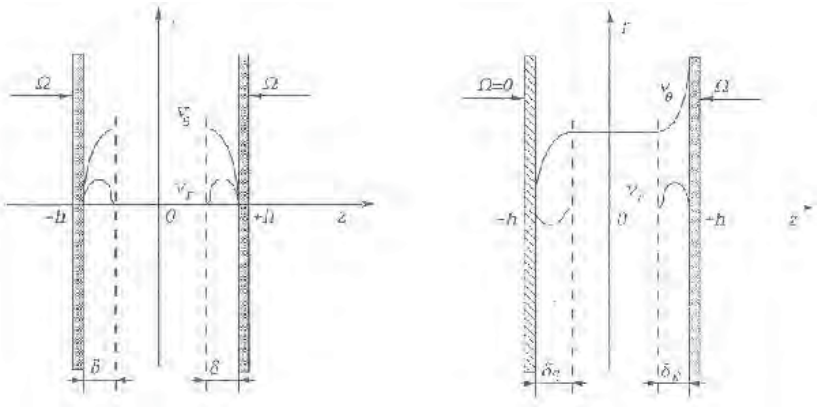

Figure 9: Sketch of the basic flows between two disks: Ekman-type flow (on the left) and Batchelor-type flow (on the right).

5 Finite geometrical configurations

Different geometries, with or without throughflow, can be investigated (see reviews in [45, 46]). In the cavity with superposed flow from outside the air may be drawn radially inward or sometimes the air flows axially through a radial clearance between the rotating disk and the hub. These configurations are relevant to practical applications in turbomachines. We note that the presence of an external flow can involve certain numerical difficulties due to the necessity to specify appropriate flow conditions on the boundaries. This can make the control of instabilities in the boundary layers more difficult by introducing uncontrolled disturbances.

In this review two configurations are investigated related to rotating disks and rotor-stator cavities. Schematics of these geometries are shown in Figure 10. The models correspond to two disks enclosing either a cylindrical or an annular domain of radial extent $\Delta R = R_1 - R_0$, where R_0 and R_1 are the internal and external radii. A cavity that includes the axis, i.e. with $R_0 = 0$, will be denoted the "cylindrical" cavity while the case $R_0 \neq 0$ will be referred to as the "annular" cavity. We note that although the annular configuration is relevant to practical applications, it is mainly used in numerical studies to investigate curvature and end-wall effects. Indeed, due to the limited scope of today's computers to effect simulations in large-size cavities (typically $\Gamma \leq 5$ in three-dimensional computations), these annular configurations allow the numerical studies of flow stability at large radii.

- The first type of cavity corresponds to a sealed rotor-stator cavity in which no air is introduced from outside. The geometrical domain is bounded by one or two cylinders of height H attached to one of the disks. One disk of the cavity is stationary (stator) and the other (rotor) rotates at uniform angular velocity $\Omega = \Omega_d e_z$, e_z being the unit vector on the axis. These geometries are relevant to fundamental investigations and correspond to those investigated in the literature in experiments (see recent works [47, 48]) as well as in numerical works (see a review in Owen [45] and, for recent works [49, 50]).

- The second type of cavity corresponds to an open rotating annulus where both disks rotate as the same speed Ω_d, and where forced flow is imposed in the radial direction. Here, the fluid enters at the inner radius and exits at the outer radius.

The only geometrical parameter in a cylindrical cavity is the aspect ratio $\Gamma = R_1/H$. In an annular cavity, the aspect ratio is defined by $L = \Delta R/H$ and an additional parameter, $R_m = (R_1 + R_0)/\Delta R$, is required for characterizing the radius of curvature.

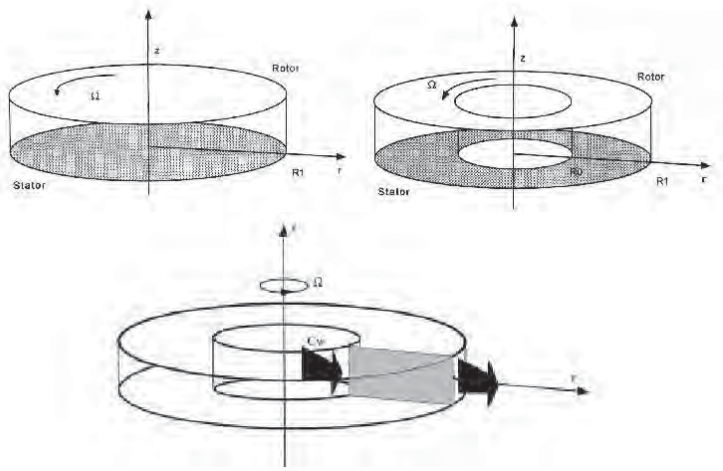

Figure 10: Geometrical models: sealed cylindrical and annular rotor-stator cavities (at the top) and rotating-disk cavity (at the bottom).

6 Mathematical model

The incompressible fluid motion in rotating cavities such as those introduced above, is governed by the three-dimensional Navier-Stokes equations that can be

written in primitive variables as below. A formulation in vorticity-streamfunction can sometimes be preferred in two-dimensional studies due to the smaller number of equations to solve (see for example in Ref. [51]). Nevertheless, we note that the lack of boundary condition on the vorticity requires specific treatments that can be costly in CPU time and memory. The scales for the dimensionless variables of space, time and velocity are $[H, \Omega_d^{-1}, \Omega_d H]$.

Along the cylindrical coordinate directions $(r,\ \theta,\ z)$ the velocity components are $(u,\ v,\ w)$, respectively, and p is the pressure. Using the above space and time scales, the dimensionless continuity and momentum equations in an inertial frame may be written:

$$\frac{1}{r}\frac{\partial\left(ru\right)}{\partial r}+\frac{1}{r}\frac{\partial v}{\partial\theta}+\frac{\partial w}{\partial z}=0,$$

$$\frac{\partial u}{\partial t}+u\frac{\partial u}{\partial r}-\frac{v^2}{r}+\frac{v}{r}\frac{\partial u}{\partial\theta}+w\frac{\partial u}{\partial z}=-\frac{\partial p}{\partial r}+\frac{1}{Re}\left[\Delta u-\frac{u}{r^2}-\frac{2}{r^2}\frac{\partial v}{\partial\theta}\right],$$

$$\frac{\partial v}{\partial t}+v\frac{\partial v}{\partial r}+\frac{vu}{r}+\frac{v}{r}\frac{\partial v}{\partial\theta}+w\frac{\partial v}{\partial z}=-\frac{1}{r}\frac{\partial p}{\partial\theta}+\frac{1}{Re}\left[\Delta v-\frac{v}{r^2}+\frac{2}{r^2}\frac{\partial u}{\partial\theta}\right],$$

$$\frac{\partial w}{\partial t}+u\frac{\partial w}{\partial r}+\frac{v}{r}\frac{\partial w}{\partial\theta}+w\frac{\partial w}{\partial z}=-\frac{\partial p}{\partial z}+\frac{1}{Re}\left[\Delta w\right];$$

where the cylindrical Laplacian operator is defined by:

$$\Delta=\frac{\partial^2}{\partial r^2}+\frac{1}{r}\frac{\partial}{\partial r}+\frac{1}{r^2}\frac{\partial^2}{\partial\theta^2}+\frac{\partial^2}{\partial z^2}.$$

Appropriate boundary conditions for the velocity components must be specified for each configuration. At the walls, no slip conditions are used. We note that the main numerical difficulty comes from the coupling between the velocity and the pressure that can be efficiently managed using a projection algorithm as in [49].

The parameters Ro and Re_δ are not known a priori and do not appear in the equations above. They can be estimated from the numerical results in order to compare with the results of Section 3.

7 Rotor-stator configuration in finite systems

Most of the studies devoted to flows between rotating disks deal with the rotor-stator configuration, which has significant relevance to many applications for industrial devices. Fundamental investigations that are relevant to the cooling of gas turbines and turbomachinery have been reported in a series of papers by Owen and Rogers [45]. These applications have motivated studies in simple generic geometries and confined configurations that model actual complex situations.

The nature and the stability of the flow strongly depends on the aspect ratio Γ $(= R/H)$ and the rotation rate. This is well illustrated in the experimental diagram

of Ref. [52] that investigated many cases over a wide range of parameters (Γ, Re_R) and that shows that the instability at the onset depends mainly on the basic steady state (see Figure 11). Other parameters may also be taken into account, such as the presence of a central hub or the end condition on the sidewall.

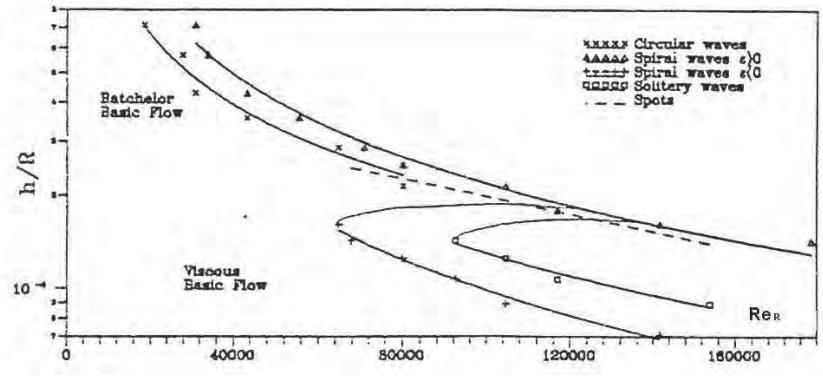

Figure 11: Transition diagram of the flow between a rotating and a stationary disk enclosed by a stationary sidewall (from [52]).

In the limiting case of a very long tube $\Gamma << 1$, the rotating disk has a vanishingly effect far from it and the flow is only dominated by the vertical-wall boundary condition.

The case of intermediate aspect ratio, $\Gamma \simeq O(1)$, and flat cavities, $\Gamma >> 1$, although much richer, lie outside the scope of this review. The investigation of the flow in rotor-stator $\Gamma \simeq O(1)$ cavities has been mainly motivated by the experimental observations of vortex breakdown. In this configuration the vortex core undergoes a sudden transition that results in a larger size and a lower velocity (including a stagnation point) and leads to the occurrence of a recirculatory bubble, Escudier [53]. The axisymmetry breaking of the basic flow gives rise to rotating waves, analysed in detail by Gelfgat *et al.* [54], Marques and Lopez [55], Blackburn and Lopez [56] and Serre and Bontoux [57] for a small value of the aspect ratio, $\Gamma = 0.25$. In spite of numerous studies, the details concerning the question of symmetry breaking have not been completely explained. The symmetry breaking could be related to the existence of asymmetric flow separation on the container wall as experimentally observed by Spohn *et al.* [58]. Three-dimensional computations of Sotiropoulos and Ventikos [59, 60] seem to confirm these observations and show that these separation lines are due to the emergence of counter-rotating pairs of spiral vortices related to Taylor-Görtler-like instability on the container wall. In contrast, for Blackburn and Lopez [56], Marques and Lopez [55] and Serre and Bontoux [57] the first bifurcation to unsteadiness is attributed to an inflectional instability of the swirling jet produced by the turning of the Ekman layer on the stationary vertical sidewall.

The limit of a very flat cavity, $\Gamma >> 1$, has been recently investigated experimentally by Cros and Le Gal [61] at $\Gamma \simeq 60$. In this limit, the fluid-layer thickness is of the same order of magnitude as the boundary-layer thickness, and the azimuthal velocity axial gradient is nearly constant and the rotating disk flow tends to be a torsional Couette type. No separated boundary layers appear even at large shear. As in Taylor-Couette flow, transition to turbulence occurs via the appearance of turbulent domains inside a laminar background and instabilities in the form of turbulent spirals, similar to the turbulent spots observed in the plane Couette or Taylor-Couette flows are reported by these authors.

In the present review, only the limit of wide gaps and high rotation rates is considered. In these circumstances, two boundary layers can develop close to the disks according to Batchelor's solution. By analogy to the case of an infinite single disk, the boundary layer close to the rotating disk is usually termed the Ekman layer, while that close to the stationary disk is termed the Bödewadt layer.

The experimental and theoretical results in the literature depict similar spatial structures in both the rotor-stator cavity and in the boundary layer on a single disk and there now exists an extensive literature on transition in these boundary layers (see Section 3). However, the stationary disk and the confining geometry have an effect on the critical Reynolds number: $Re_{\delta c}$ is noticeably increased with respect to the standard Ekman configuration. Indeed, [62] estimated $Re_{\delta cII} = 85.3$ and $Re_{\delta cI} = 281$ for their experimental apparatus. Also, Sirivat [63] studied the dependence between the basic flow and the instability and obtained experimentally a stability diagram using as the parameter space the gap width and the Reynolds number. In this stability diagram the basic flows and the characteristic of the subsequent instabilities are represented (i.e. the critical Reynolds number and the spatial and temporal features of the instability near the onset). The experimental observations and works of Schouveiler *et al.* [48] and Gauthier *et al.* [47] have extensively covered the phenomena that appear in this diagram. Two classes of instability have been observed, axisymmetric propagating vortices and positive spirals, characteristics that have been further explored in numerical studies by Serre *et al.* [49].

7.1 Base flows

The base-flow solution is steady, axisymmetric, and is composed of boundary layers on each disk and a central core flow in near solid-body rotation. These basic-flow solutions have been displayed by Serre *et al.* [49] for two configurations one of which includes a hub. These are displayed here in Figure 12. The two disjoint boundary layers behave virtually independently of each other, with fluid pumped radially outward along the rotating disk and radially inward over the stationary disk. These boundary layers are separated by the rigidly rotating core where the azimuthal component of velocity is independent of z (see Greenspan [11]).

As was mentioned in Section 4, the main effect of the finite radius of the disks is that the solutions do not satisfy self-similarity although there was a qualitative resemblance over a large region far away from the end walls [42]. Despite this, they are still usually referred to in the literature as of Batchelor type.

The deviation between similarity solutions and finite-disk flows can be illustrated by comparing the values of the solid-body angular velocity at mid-height, $v^*(z=0)$, normalised with the local angular velocity of the rotating disk. These values define Rossby numbers Ro, $Ro = v^*/\Omega r^*$ that link the rotation speed of the disk and the thickness scale of the Bödewadt layer, $\delta_B = (\nu/\Omega_f)^{1/2}$, as $v^*(z=0) = \Omega_f r^*$. For infinite disks at sufficiently large rotation rates, laminar similarity solutions give a constant $Ro = 0.313$, as theoretically determined by [62] for $Re = 1000$. Unlike the similarity studies, Serre *et al.* [49] for a cylindrical cavity ($L = 2$, $Re = 1400$) observed a radial variation of the Rossby number Ro and its value at the center of the cavity is in this case 0.53, that is about, 70% larger than the value predicted by the similarity studies. A comparison with available values of Ro in confined and non-confined geometries can be found in Randriamampianina *et al.* [64]. An analytical expression for Ro as a function of radius is proposed in [45].

In spite of this deviation between similarity solutions and finite-disk flows, the results provided by Brady and Durlofski [42] indicate that, for moderate-to-high Reynolds number flows, the similarity solution may be useful as an approximation to the actual flow, specially in the flow region located far from the end wall, but not as a quantitative description of the flow; such a description requires experiments and/or computations.

The core-fluid rotation rate increases from the shaft to the shroud as noted in [64]. Serre *et al.* [49] (numerically) and Gauthier *et al.* [47] (experimentally) have shown that this expansion of the core with the radius corresponds to a linear decrease of the Bödewadt layer thickness from the shaft to the shroud. A linear fit of the results of [47] gives

$$\delta_B/\delta_0 = 6.9 - 5.3\,(r^*/R_1)\,,$$

where $\delta_0 = (\nu/\Omega)^{1/2}$ as the leading order dependence of the Bödewadt layer thickness on radius in the middle region of the cell. Such behavior of the base flow in confined geometries means that the radial flow is non-parallel (as is clearly shown in Figure 12 at the bottom) and thus the description of the instability and the comparison with linear stability analysis require local scaling parameters. Nevertheless, it is expected that the parallel-flow assumption has no large influence on numerical results and that general instability characteristics do reveal the general features of the flow. For example, using linear-parabolised stability theory including non parallel effects, Fernandez-Feria [65] obtained a critical Reynolds number of the Bödewadt-layer Type II instability (single disk), at $Re = 19.8$, very close to that obtained numerically by Serre *et al.* [24] in a cylindrical cavity $\Gamma = 5$, $Re = 18.9$. Even if non parallel effects due to radial confinement could explain the slight disagreements observed between linear stability analysis and numerical results, the parallel-flow studies provide qualitatively correct descriptions of the investigated class of flows and are very helpful in interpreting DNS results in terms of Type I and Type II instabilities and in determining the absolute/convective character of the boundary-layer flow.

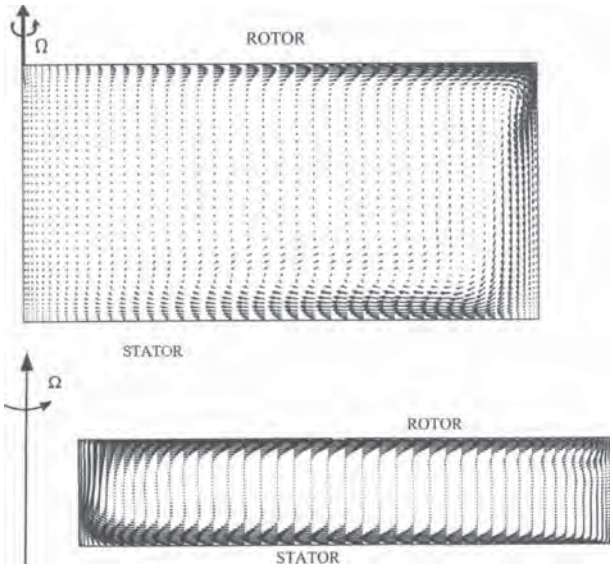

Figure 12: Basic flows in rotor-stator: in cylindrical cavity at $Re = 1400$, $\Gamma = 2$ (at the top) and in annular cavity at $Re = 200$, $L = 5$ (at the bottom). Velocity field in the plane (r, z, $\pi/4$) (from Serre *et al.* [49]).

7.2 Instabilities and transition

The primary destabilisation of the flow occurs in the Bödewadt layer as expected from the linear stability analysis.

7.2.1 Axisymmetric vortices

Propagating axisymmetric waves were first observed in a cylindrical tank ($\Gamma = 0.5$) under transient conditions, only during an impulsive spin-down to rest, by Savas [35] experimentally (see Figure 13b) and then Lopez and Weidman [66] and Lopez [36], both numerically (with an axisymmetric code) and experimentally. In the rotor-stator case and for experimental permanent conditions, the existence of axisymmetric structures have been mentioned in San'kov and Smirnov [44] and axisymmetric vortices propagating in the Bödewadt layer have been described only recently by Schouveiler *et al.* [67, 48] and in Gauthier *et al.* [47] (see Figure 13a. Such structures have also been reported numerically by Cousin-Rittemard *et al.* [68] (with an axisymmetric code) and further by Serre *et al.* [49] using fully three-dimensional computations.

Schouveiler *et al*. [67, 48] reported an axisymmetric time-dependent instability inside a Batchelor flow at $Re = 222$ for $\Gamma = 8.74$: there five pairs of corotating circular rolls (RC) appear close to the outer cylindrical wall and travel inward. Schouveiler *et al.* [67, 48] also showed that the angular frequency decreases from $\sigma = 3$ (in a region close to the external wall) down to $\sigma = 1$ near the axis, certainly

due to pairing phenomena, as observed by Cousin-Rittemard in a 2D simulation [68]. We notice that no such dislocation phenomena have been observed by Gauthier *et al.* [47] nor in the 3D simulations of Serre *et al.* [49]. The most detailed study of the primary instability leading to these propagating axisymmetric waves has certainly been carried out by Gauthier *et al.* [47] in a cylindrical cavity of aspect ratio $\Gamma = 20.9$. These authors have shown that this instability has all the properties of a supercritical bifurcation (with the most unstable frequency $\sigma = 4$) with a threshold at $Re_c \simeq 75$ and that above Re_c, the instability is linearly convective leading to a high sensitivity to external controlled or uncontrolled forcing.

Serre e*t al.* [49] also extensively studied this mode of instability in both annular and cylindrical cavities. In a cylindrical cavity $\Gamma = 2$, the solution is shown in Figure 14 at $Re = 4000$. Their solutions are characterized by three to five pairs of circular vortices depending on the geometry, occurring over the shroud and travelling in the main flow direction. The wavelength of these corotating circular rolls can be measured by experimental or numerical visualisation. Schouveiler *et al.* [48] obtained a dimensionless wavelength $\lambda/\delta \simeq 15$ in agreement with the observations of Savas [69] and Gauthier *et al.* [47] ($\lambda/\delta \simeq 12.5$ for the most unstable mode) and with the calculations of Fernandez-Feria [65]. Serre *et al.* [49] specified that the wavelength increases with radius and could vary over the range of $15 \leq \lambda/\delta \leq 25$ certainly due to the non-parallelism of the Bödewadt flow, as previously mentioned. In the cylindrical cavity (with no hub) the structures travel in the Bödewadt layer only to a final radius corresponding to a local Reynolds number $Re_\delta = 21$ ($\Gamma = 2$, $Re = 4000$) and $Re_\delta = 27$ ($\Gamma = 5$, $Re = 1600$), [49] in quite good agreement with the experimental results of Savas [35] ($\Gamma = 0.5$, $Re_\delta = 35$) and linear stability results of Fernandez-Feria [65] in the Bödewadt layer ($\Gamma = 5$, $Re_\delta = 19.8$). In the annular cavities, axisymmetric vortices are also visible in the rotating-disk boundary layer but the amplitude is much weaker. As the rotor is expected to remain stable at the considered rotation rates ([3, 24]), the structures in the Ekman-layer seem to be produced by the perturbation induced by the Bödewadt-layer instability. Nevertheless, the spatio-temporal characteristics of these structures are relevant to Ekman layer instabilities that will be discussed in the next section; a case for a rotating cavity with a radial throughflow.

In good agreement with experiments ([67, 48] [47]) the frequency of the numerical solutions evolves from $\sigma \simeq 1$ ($\Gamma = 2$) ([68, 49]) to $\sigma \simeq 4$ ($\Gamma = 5$) ([49]). Note also, that in the case of a fluid rotating over a single stationary and infinite disk, Lingwood [4] found theoretically $\sigma = 1.3$ at the convective/absolute transition for the axisymmetric structures in the Bödewadt layer. A supercritical Hopf bifurcation from a Batchelor steady state to a periodic flow has been firstly observed numerically in the short cavity $\Gamma = 2$ ([68, 49]) and more recently in the larger $\Gamma = 5$ cavity ($11500 < Re_R < 12300$, Serre *et al.* [24]). Surprisingly, no Hopf bifurcation from a steady Batchelor state to an unstable oscillatory flow had been numerically reported prior to the paper of Serre *et al.* [24], except for cavities of small aspect ratio $\Gamma = 2$ (See refs. [68, 49]). The main reasons seem to be related either to the axisymmetry hypothesis of the computations [70] either from the use of a rotating end wall (stabilizing the flow coming from the rotating-disk layer) in

contrast to experiments or to the use of supercritical condition as in Serre *et al.* [49]. Critical Reynolds numbers of the different studies have been summarized in Figure 17 of the paper of Serre *et al*. [24].

Simulations and experiments exhibit the same axisymmetric mode of instability of the Bödewadt layer. Stability analysis of Fernandez-Feria [65] and Pikhtov and Smirnov [34] apparently recognized this mode as a Type II instability. Numerical simulations of Tuliska-Sznitko *et al.* [71] and experiments of Schouveiler *et al.* [67, 48] confirm this point.

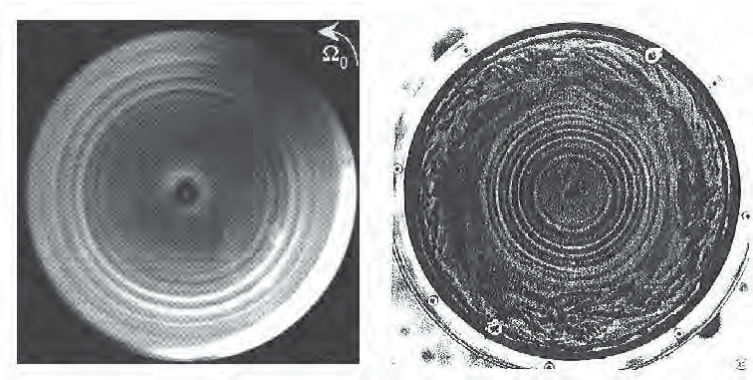

Figure 13: Visualizations of experiments showing circular patterns related to Bödewadt-layer instability. On the left side, experiments of Gauthier *et al.* [47] at constant rotation of the disk. On the right side experiments of Savas [35] during spin-down.

7.2.2 Spiral vortices

At higher values of the Reynolds number, another unstable mode is observed in the Bödewadt layer ([23, 48, 49]). At quite small values of aspect ratio (typically $2 \leq \Gamma \leq 20.5$) this secondary instability creates a spiral-wave pattern that can coexist at the lowest rotation rates with the previous circular waves. Spirals appear at the periphery and circles are then only observed closer to the center. The visualizations of Figure 15 show the coexistence with circular rolls of the co-rotating spiral rolls either in the periphery of the system or in the central area. Serre *et al.* [49] have shown that this axisymmetric instability is robust and coexists with the three-dimensional spiral instability when the mean curvature is large, *i.e.* at small radii in the cylindrical cavity, when the radial confinement is sufficiently weak (for example $\Gamma = 5$). On the other hand, the axisymmetric instability is unstable to azimuthal disturbances when the curvature is small, *i.e.*, at large radii in the annular cavity ($R_m = 5$). The axisymmetry of the flow is thus broken by this second bifurcation. These spirals roll up in the direction of the rotating disk with an angle ε of about 25° and the flow exhibits typically a spiral pattern with a number of

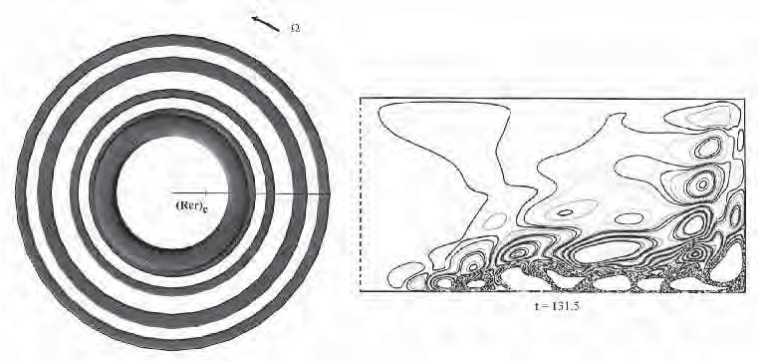

Figure 14: Circular patterns related to Bödewadt-layer instability in a cylindrical cavity at $\Gamma = 2$ and $Re = 4000$. On the left, isosurface of vertical velocity. On the right, isolines of vertical velocity in the meridianal plane (r, z). Three-dimensional DNS results from Serre *et al.* [49]

arms in the range $[16 - 30]$ depending on the value of the aspect ratio and the rotation rate. Serre *et al.* [49] obtained a similar solution for the $\Gamma = 5$ cylindrical cavity and observed that the angle of the spiral arms was not constant but varied with radius in the range $7° \leq \varepsilon \leq 28°$.

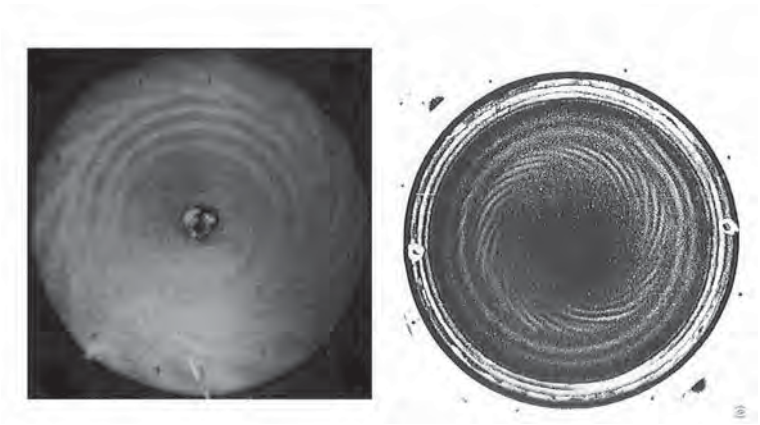

Figure 15: Flow visualization of experiments showing the coexistence of circular and spiral patterns related to Bödewadt-layer instabilities. On the left, experiments of Schouveiler *et al.* [67] at constant rotation of the disk. On the right, experiments of Savas [35] during spin-down.

A pure spiral pattern was also observed numerically and experimentally at higher Reynolds numbers. As in the axisymmetric case, the disturbances vanish

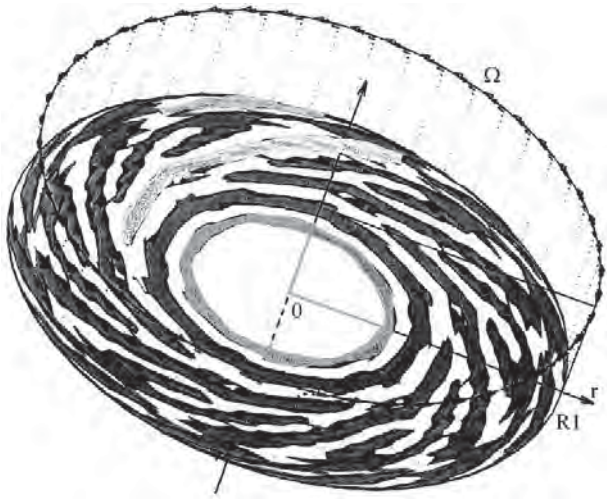

Figure 16: Coexisting circular and spiral patterns related to Bödewadt-layer instabilities in a cylindrical cavity at $\Gamma = 5$ and $Re = 1200$. Isosurface of vertical velocity. Three-dimensional DNS results from [49].

at a radius corresponding to a Reynolds number of about $Re_\delta = 27$.

Unlike the circular waves previously described, their frequency does not appear to be locked to the disk rotation frequency and varies from $1.7 \leq \sigma \leq 4$ .We notice that at larger aspect ratios (typically $21 \leq \Gamma \leq 100$), experimentalists ([48]) also observed stationary spiral arms with positive angles too ($12 \leq \varepsilon \leq 15$) but not related to boundary-layer instability as they take up the entire height of the cavity.

For the annular cavity (Figure 17), the disturbance produced by the supercritical instability of the stator layer is transmitted along the shaft to the rotor and brings about a subcritical instability in the Ekman layer [49]. Spiral arms are also visible in the Ekman layer of the rotating disk but in contrast to the stationary disk layer, the angle of the spiral arms is negative, decreasing dramatically between the inner and the outer radii, ranging from $-7.5^\circ \leq \varepsilon \leq -20^\circ$. As for the circular patterns, the characteristics of these structures are found to be in good agreement with the Type II instability of the Ekman layer, which will be discussed in detail in the next section.

One extensive study of these spiral patterns has been carried out by Schouveiler *et al.* [48]. In particular they showed that the wave number selection process of this secondary instability could be described as a result of the Eckhaus instability that selects the number of spiral arms as illustrated in Figure 18. At threshold, the number of rolls is 18, but depending on the initial conditions of the flow, states with 16 to 24 arms can also be obtained.

The analysis of San'kov & Smirnov [44] of the Bödewadt layer can be favourably compared with the experimental and numerical results and recognizes this spiral mode of positive angle as a Type I instability.

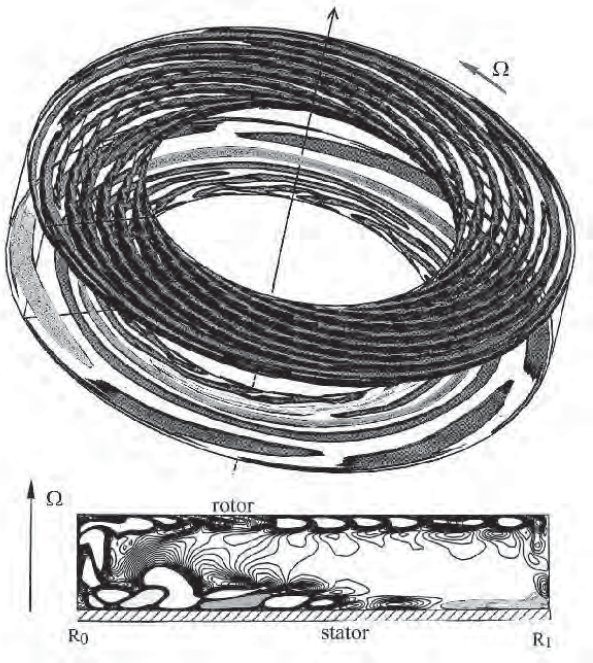

Figure 17: Spiral patterns related to rotating and stationary-disk boundary layers at $Re = 400$ in an annular rotor-stator cavity ($Rm = 4$, $L = 5$). At the top 3D visualization of isosurface of the vertical component of the velocity. At the bottom, isolines of vertical component of the velocity in the meridional plane (r, z). DNS results from Serre *et al.* [49].

8 Rotating annular cavity with radial forced flow

The configuration used by experimenters to study the stability of the Ekman boundary-layer flow consists of an incompressible fluid filling a rotating cylindrical container, the cylindrical annular walls are 'open' i.e. they are no radial barriers but there are a source of flow at the inner annulus and a sink at the outer annulus or vice versa ([73, 25, 26, 28]). This configuration is usually named the source-sink configuration. In these flows, the fluid outside the boundary layer does not have a constant angular velocity and both Rossby and Reynolds numbers depend of radius and both increase with decreasing radius. Thus, in these flows the Rossby number is not strictly equal to zero and these configurations can be referred as to "low Rossby number experiments" ([4]). Nevertheless, the results presented for the Ekman layer in section 3.1 at $Ro = 0$ remain applicable here. The rotating flows in the source-sink configuration have also been extensively studied by Owen *et al.* (see references in Owen and Rogers [46]) because of its relevance to certain turbomachinary flows. They studied experimentally and numerically, using

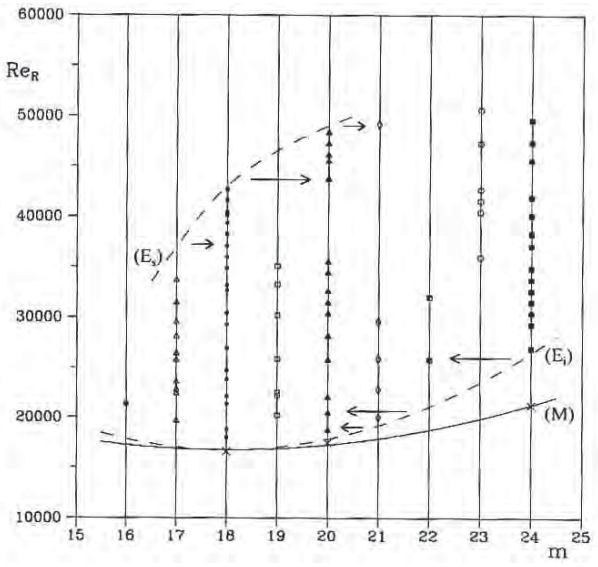

Figure 18: Stability of the spiral modes of wave number m in a cylindrical rotor-stator cavity of aspect ratio $\Gamma = 8.75$. (M) Marginal stability curve; (Es) and (Ei) upper and lower limits of the Eckhaus instability (from Schouveiler [72]).

two-dimensional simulations transition to turbulence. The turbulent flows were investigated by fixing the rotation rate and increasing the mass flow rate. Depending on the configuration, the instabilities may be observed in the entry flow and also in the boundary layers, where patterns with similar characteristics to the Type I and Type II instability can be observed. An illustration of these experimental investigations is shown in Figure 19 for two values of mass-flow rate. At moderate mass-flow rate, the flow is laminar and smoke can be distinguished in the four flow regions (white zones) as analytically predicted by Hide [74] (see below in the next section). At large mass flowrate, the flow is turbulent and the flow axial symmetry with respect to the mid-height plane is broken. Smoke fills almost the whole cavity and is entered in the core flow. Thus, the flow-structure model proposed by Hide [74] is therefore inappropriate at large mass-flow rate.

In this section we mainly present a synthesis of recent numerical results of unsteady flows showing circular and spiral patterns, principally reported in Crespo del Arco *et al.* [51] and Serre *et al.* [75].

8.1 Base flow

The flow is axisymmetric and four separated regions can be distinguished: the entry and exit zone, the core and the boundary layers. The velocity profile in the middle-radius region is similar to the Ekman profile given in section 3.1 and pre-

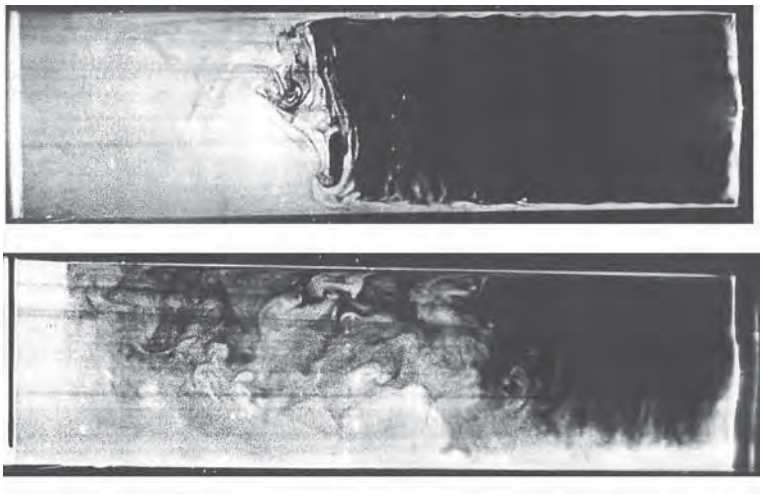

Figure 19: Visualizations with smoke (white zones) showing the structures of the flow between two rotating disks in laminar (above) and turbulent regime (below) (from Owen and Rogers [46]). The rotation axis stands on the left.

sented in eqn. (3). The configuration is sketched in Figure 10. A constant mass-flow rate (positive if the flow is outwards), Q, is imposed at both inner and outer cylinder surfaces that is made dimensionless, $C_w = Q/\left(2\pi\nu H\right)$. The forced flow induces a core velocity which can be written

$$V_\infty \; r = -C_w Re^{-1/2}, \tag{5}$$

relative to the velocity of the disk. The flow in the core is not geostrophic as it is assumed in models and prototypes of meteorological conditions since it is not the result of the balance between Coriolis force and the stress tensor. The asymptotic expression for the velocity flow field was obtained by Hide [74], and some quantitative corrections of the magnitude of the core velocity (5) are provided in some subsequent papers (see Owen and Rogers [46] for references).

The control parameters, the Reynolds and Rossby numbers, may be estimated from the relationships (5),

$$Re_\delta = \frac{|V_\infty^*|\,\delta}{\nu} = \frac{C_w}{r},$$
$$Ro = \frac{|V_\infty^*|}{\Omega r^*} = \frac{C_w}{Re^{1/2}}\frac{1}{r^2}.$$

We notice that in contrast to the infinite-disk approximation in section 3.1 non-linear terms can be important. Thus, linear stability results would only be reached in the linear limit, i.e. for $Ro_\delta << 1$, but can be nevertheless used as a reference.

Moreover, the flow is not parallel because the velocity at the core in eqn. (3) is not uniform in the radial direction. Thus, the term 'Ekman boundary layer' is not strictly applicable but will be, nevertheless, used to conform with previous usage.

The axisymmetric flow was computed numerically by Crespo del Arco *et al.* [51]. An illustration of the basic flow obtained numerically using a parabolic entry and exit flow is shown in Figure 20, showing the streamlines of the steady flow at $C_w = 119$ and $Re = 446$. The qualitative agreement with experimental visualizations in the laminar regime, shown in Figure 19, is good. The steady velocity field obtained by Crespo del Arco *et al.* [51] (Figure 21) is also in very good agreement with the asymptotic solution of [74]. The four different zones obtained by Hide [74] are clearly visible in both these figures.

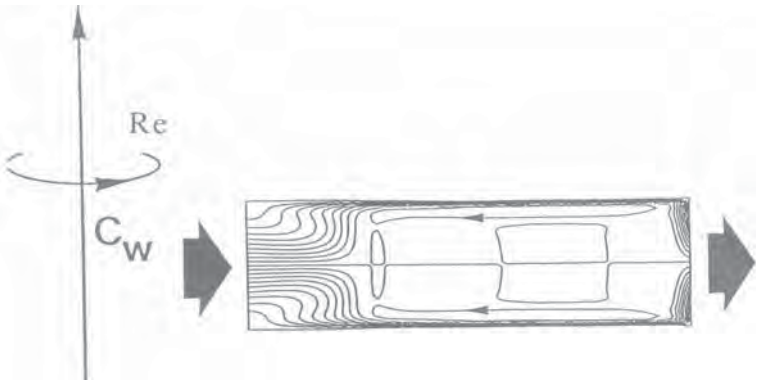

Figure 20: Streamlines for steady flow for $Cw = 119$, $Re = 446$, $Rm = 1.22$, and $L = 3.37$ (from Crespo del Arco *et al.* [51]).

8.2 Instabilities and transition

The transition to chaotic motion reveals a first transition to oscillatory motion associated with the onset of waves in the boundary layers. The three-dimensional Navier-Stokes equations provide a complex scenario with hysteresis and multiple stable solutions with spiral waves in the boundary layers and with different azimuthal wave numbers and frequencies.

8.2.1 Axisymmetric patterns

The unstable flow in this source-sink configuration was observed experimentally by Arons *et al.* [73] who described the pattern in the flow as 'almost perfectly concentric cylindrical sheets or curtains of water which rise as sharply defined vertical jets from the Ekman layer and penetrate the entire depth of fluid'. A flow solution with a similar circular pattern has been obtained by Serre *et al.* [75] at $C_w = 1705$ and $Re = 446$ ($84.4 \leq Re_\delta \leq 126.5$) using three-dimensional

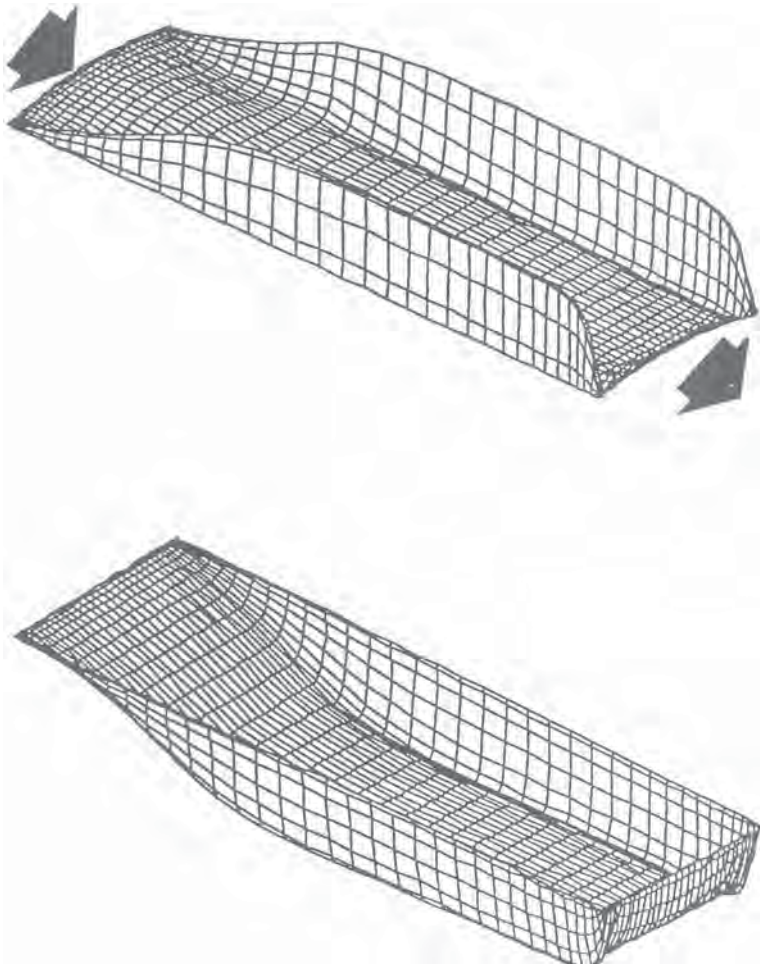

Figure 21: Two-dimensional radial and azimuthal velocity plots: $u \times r$ and $v \times r$. $C_w = 119$, $Re = 446$, $R_m = 1.22$, and $L = 3.37$. (from Crespo del Arco *et al.* [51]).

computations of the time-dependent Navier-Stokes equations. The initial condition for this computation was the steady solution at $C_w = 1288$ ($64 \leq Re_\delta \leq 95$) and $Re = 446$ computed using the velocity profiles in eqn. (3) with a geostrophic velocity given by eqn. (5) as inflow and outflow boundary conditions. Transition to an oscillatory flow occurs when the mass flow rate is increased to $C_w = 1705$. The unsteady flow remains axisymmetric and exhibits circular patterns in both layers (Figure 22). In the meridional plane, counter-rotating rolls travel radially outwards.

As the axial component of the velocity is zero in the basic flow, the contour

lines can be used to emphasize the perturbations about the basic flow. The angular frequency of the flow is $\sigma = 7.4$, (scaled with the angular rotation rate) and is related to the outward-travelling wave. Its value is in good agreement with the values reported from experiments by Caldwell and Van Atta (1970), at higher values of the Reynolds number. For Re in the range of $110 < Re_\delta < 250$, these authors reported a linear dependence of the frequency, $7 < \sigma < 12$.

We finally note that similar circular patterns have only been observed experimentally in a similar configuration in the work of Arons *et al.* [73], but have often been reported in experiments related to the Bödewadt boundary layer (Section 7), see for example the works of Wilkinson and Malik [30]; Savas [35] or Gauthier *et al.* [47].

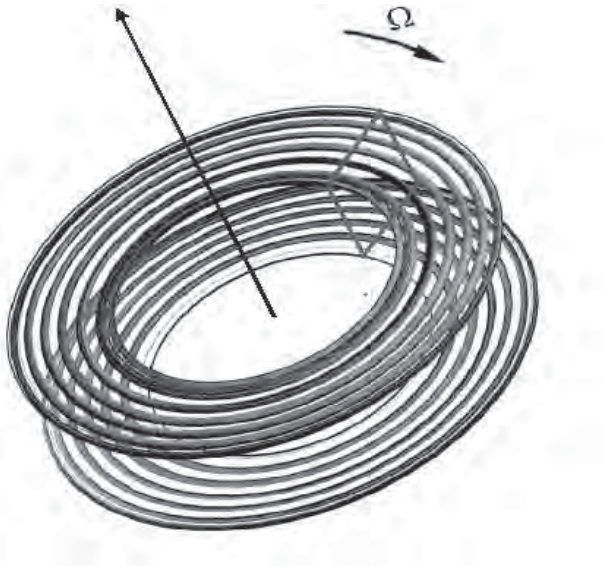

Figure 22: Annular patterns related to an axisymmetric mode of Type II instability of the Ekman layer, (from Serre *et al.* [75]).

8.2.2 Three-dimensional spiral patterns

Three-dimensional spiral patterns related to Type I and Type II instabilities of the Ekman layer have been observed in experiments (see the review in Faller [5]). Type II and Type I have the form of spiral vortices but of the opposite angle relative to the geostrophic velocity and with a lower value of critical Reynolds number (see Table 2).

In the Ekman-layer experiments, the Type II instability only appeared when there were mechanical disturbances in the experiment, while the numerical studies [51, 75] showed vortices that can be more related to Type II than a Type I instability

over the range of Re_δ considered. The experimental results of refs. [15, 76] as well as the numerical results of Ref. [75] showed that spiral arms have a negative angle over a range of about $-20^\circ \leq \varepsilon \leq -5^\circ$ and a wavelength in a range $22 \leq \lambda/\delta \leq 33$, slightly varying with the radial location. Faller and Kaylor [15] and Serre *et al.* [75] observed spiral arms, the former for a critical Reynolds number $Re_\delta \simeq 70$ and the latter at a slightly larger value, $Re_\delta = 85$. These characteristic parameters are in good agreement with stability analyses of Faller [5] for $Ro = 0$ who obtained Type II instability characterized by spiral arms of wavelength $\lambda/\delta = 20.1$ and forming an angle $\varepsilon = -23.1^\circ$ (see Table 2).

Serre *et al.* [75] obtained multiple nonlinear stable solutions with different numbers of spiral arms, by disturbing the axisymmetric solution (at $C_w = 1705$) with small perturbations of different wave numbers. Figure 23 shows three solutions of spiral instability patterns obtained at the same Reynolds number, $C_w = 1705$. The numerical study of [75] accurately investigated the time behavior of these spiral patterns. All three-dimensional solutions have been found to be periodic with a frequency slightly larger than for the axisymmetric solution with a circular pattern.

The dispersion relation $\sigma = \sigma(n)$ between the frequency and the azimuthal wave number shows a linear increase of the frequency with wave number. Crespo del Arco *et al.* [51] as well as Serre *et al.* [75] showed that the phase velocity of circular waves behaves as (r^{-1}) and that the spiral wave fronts propagate in the azimuthal direction with dimensionless angular velocity $\omega = \sigma n^{-1}$. Consequently, the velocity of the wave front can be written as $(v_{\Psi r}, v_{\Psi\theta}) = \left(Ar^{-1}, \omega r\right)$, where A is a constant. A generic equation of the wave front has been proposed in Ref. [75], derived from the condition of colinearity between the displacement of the instability and the phase velocity, expressed as

$$r^2 = \frac{nLR_m}{3\pi}\left(\theta + \frac{2i\pi}{n}\right), 0 \leq i \leq n-1.$$

This hysteresis, where the final stable patterns may be characterized either by a purely radial wave number or by other wave numbers with radial and azimuthal components, are strongly reminiscent of the zig-zag instability in Rayleigh-Bénard convection.

9 Turbulent flows

Most of the studies devoted to turbulent rotating flows concern the shear-driven boundary layer induced by a rotating disk in an otherwise quiescent fluid. The mean flow develops substantial skewing across the boundary layer, with a cross flow that reaches about 11% of the local disk speed, so that three-dimensional effects are important. Indeed, the disk boundary layer is one of the simplest platforms for investigating the underlying structure of three-dimensional boundary layers. Most extensive experimental investigation of the statistical and structural features of the 3D boundary layer near a rotating disk is certainly that of Eaton's group at Stanford [77]. A key feature of their studies concerned the modification of

boundary-layer turbulence by crossflow. A complementary large-eddy simulation has been carried out by Wu and Squires [78].

Another key point in such flows is the identification of the mechanisms responsible for transition that would improve the prediction methods and could lead to new and efficient control strategies. Despite intensive work and recent advances (see [79, 80, 81]) no full understanding of the turbulent breakdown process has yet been achieved, especially in regard to nonlinear behaviors. As we already mentioned in Section 3, absolute instability is now recognised to play a fundamental role in the transition to turbulence in the flow over a rotating disk ([2, 3, 8]).

Compared to the laminar flows considered above, the turbulent rotor-stator flows have been the subject of fewer investigations due to the experimental and numerical technical difficulties of investigating these regimes. One of the first experimental and theoretical studies of turbulent flows in rotor-stator systems was carried out by Daily and Nece [82] who identified four flow regimes of which two are turbulent characterized by merged or separated boundary layers depending on the value of the aspect ratio and the Reynolds number. More recently, Itoh *et al.* [62] and Cheah *et al.* [83] carried out very careful experiments and measured the mean velocity distribution as well as the Reynolds stress tensor. These authors mainly showed that a characteristic of the rotor-stator flow with non-merging boundary layers is that the turbulence occurs first along the Bödewadt layer that is found to be noticeably less stable than the Ekman rotating layer. Mean velocity profiles measured in experiments by Cheah *et al.* [83] at $Re_R = 3 \times 10^5$ and $Re_R = 1.6 \times 10^6$ are displayed in Figures 24 and 25 at different radial positions. These data show that the mean flow is of the Batchelor type as in a laminar regime. At $Re_R = 3 \times 10^5$ the Ekman layer is still laminar or transitional, while both layers are turbulent at $Re_R = 1.6 \times 10^6$. In a cavity of aspect ratio $\Gamma = 12.5$, Itoh *et al.* [62] found that the rotor layer was laminar for a local Reynolds number of $Re_r = 1.6 \times 10^5$ ($Re_r = \Omega r^2/\nu$), turbulent for $Re_r = 3.6 \times 10^5$ and fully turbulent for $Re_r = 4.6 \times 10^5$, while the stator layer becomes turbulent at much lower Re_r. Thus, the structure of these flows is highly complex, involving laminar, transitional and turbulent flow regions.

These flows are thus very challenging for complete 3D numerical approaches requiring very fine meshes to integrate the fully time-dependent Navier-Stokes equations until a statistically stationary state is reached (DNS). Thus, there are at present only a few DNS results. Due to the simultaneous improvement in algorithms and computing resources, however, DNS has now become a powerful and reliable tool to investigate the turbulent-flow regime. Indeed, DNS can make and has made a significant contribution to the improvement of turbulence models by providing accurate instantaneous quantities that help clarify the intrinsic flow structures associated with turbulent rotating flows. Moreover, the numerical data can be averaged so as to provide target turbulence data for any subsequent modelling attempts at reproducing the flow.

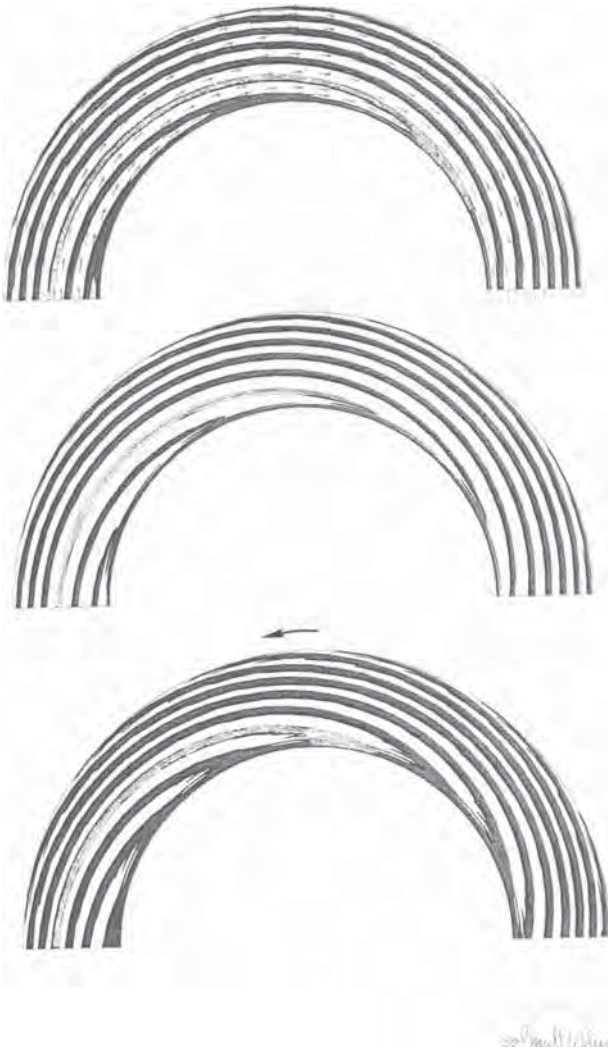

Figure 23: Three-dimensional solutions of instantaneous iso-surface of the axial velocity component, for $0 < z < 1$, projected on the plane $(r, \theta, z = 0)$; $C_w = 1705$, $Re = 446$ and at $R_m = 5$, $L = 3.37$. The cavity rotates in the anti-clockwise direction. Spiral patterns of the instability with six arms, and velocity field in the geostrophic region (top). Spiral patterns with eight arms (middle). Spiral patterns with 12 arms (bottom) (from Serre *et al.* [75].

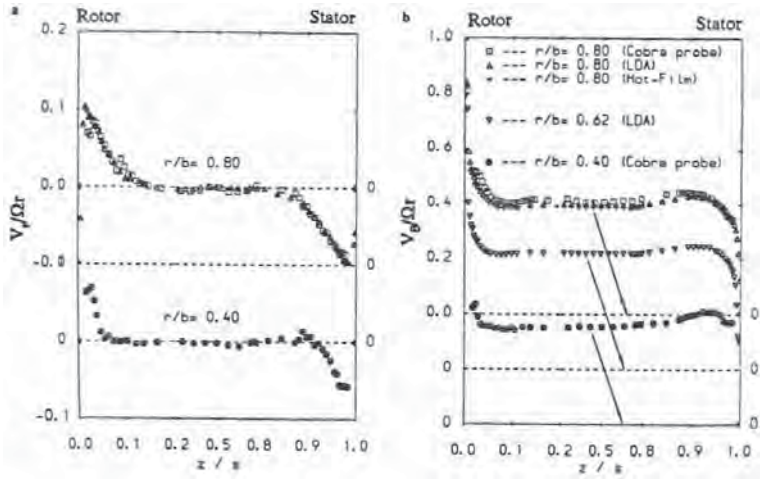

Figure 24: Mean velocity profiles at $Re_R = 1.6 \times 10^6$. (a) radial; (b) circumferential (from Cheah *et al.* [83]).

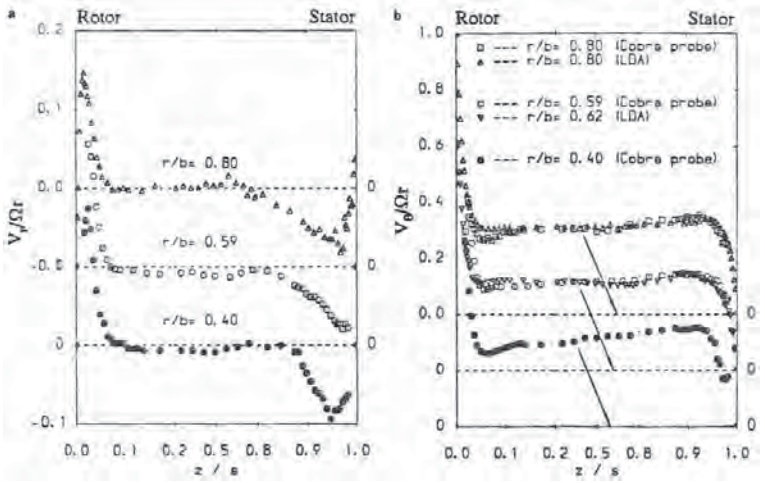

Figure 25: Mean velocity profiles at $Re_R = 3. \times 10^5$. (a) radial; (b) circumferential (from Cheah *et al.* [83]).

Pao [84] conducted one of the first numerical investigations into flow in a rotating cavity, considering the problem of a stationary disk housed in a rotating casing. The highest rotational Reynolds number for which convergence was achieved was only $Re = 200$. Today, using high-performance supercomputers, direct numerical simulation (DNS) of flows between a rotating and a stationary disk can be performed to about $Re = 4 \times 10^5$ ([85]), very close to the fully turbulent Reynolds number of the rotating-disk layer experimentally observed by Itoh *et al.* [62]. Lygren and Andersson [85] simulated flows between infinite disks with local gap ratio $H/r = 50$ using a second-order finite-difference scheme and imposing periodicity in both azimuthal and radial directions, arguing that the turbulence statistics vary relatively slowly in the radial direction, except near the transition ([62, 77, 83]). The main motivation of the study of Lygren and Andersson [85] was to explore the modification of the turbulence due to three-dimensionality of the mean flow. One of the key points of this work was the investigation of coherent structures near both disks that had been proposed to explain experimentally observed phenomena - notably, the 'bursting' process (responsible for most turbulence production near the wall and thus increased turbulent drag and mixing) - in turbulent boundary layers. These structures were found to be remarkably similar adjacent to both the stationary and the rotating disk despite the difference in the origin of the crossflow on the two disks. Moreover, the numerical results showed that the sweeps generated by the vortices are much weaker than the ejections, which is different from those is found in a turbulent channel flow ([86]). Lygren and Andersson [85] identified coherent structures in both layers in order to provide sufficient information regarding the roles played by sweeps and ejections in shear-stress production. Aligned and tilting outward elongated structures (with respect to the tangential mean velocity) have been identified by means of the λ_2 criterion by Lygren & Andersson [85] showing an effect of the crossflow. (Jeong and Hussain [87] define a vortex as a connected region of negative λ_2, which is the second largest eigenvalue of the tensor $s_{ik}s_{kj} + r_{ik}r_{kj}$ where $s_{ij} \equiv (u_{i,j} + u_{j,i})/2$ the strain rate and $r_{ij} \equiv (u_{i,j} - u_{j,i})/2$ the rotation tensor.) Figure 26 displays these two types of vortices near the rotating disk.

In the case of flows between finite disks, Jacques *et al.* [88] carried out a two-dimensional "DNS" at $Re = 10^6$ using a second-order finite-difference technique, while in three-dimensional DNS (periodic in the azimuthal direction and non-homogeneous in both the axial and radial directions), computer limitations only permit, at present, the simulation of transitional turbulent cavity flows to $Re = 3 \times 10^5$ ([89, 90]). Serre *et al.* [89, 90] carried out a DNS using a highly accurate pseudo-spectral Chebyshev-Fourier method, in two annular enclosed rotor-stator cavities of aspect ratio $L = 2.3$ and 4.72 and obtained a qualitative agreement with experiments at higher Reynolds numbers.

As observed in experiments ([83, 62]), these two- and three-dimensional computations show marked differences between the Ekman and Bödewadt layers, laminar and turbulent flows coexisting within the cavity. An analysis of the instantaneous field reveals large-scale vortices travelling inside the stator layer. In three-dimensional computations, these vortices extend in rings and, at smaller radii, in

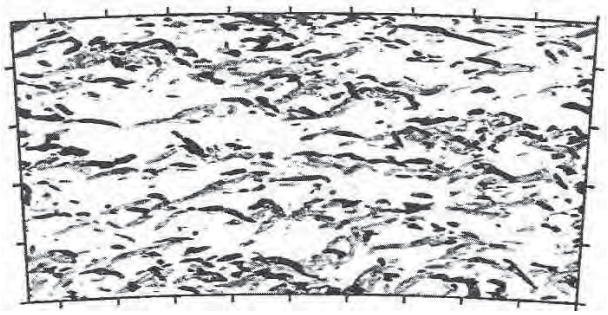

Figure 26: Isosurface plot (top view) of $\lambda_2 = -0.002$ in the region $0 < z^+_{rel} < 50$ near the rotating disk. Light (dark) shading represents Case 1 (Case 2). The tangential mean velocity in the rotating coordinate system is from left to right (from Lygren and Andersson [85]).

spiral arms, in the tangential direction (Figure 27). Serre *et al.* [89] also underlined the effects of the end walls on the turbulent flow with a large number of vortices of different scales near the stationary shroud and rotating inner shaft. The statistical results show that there exists on average a primary flow in the tangential direction coupled with a secondary flow in the meridional plane. The statistical data display, near the fixed disk, a very strong anisotropy in the normal stresses that is typical of low Reynolds number wall flows. As would be inferred from a stress budget, the intensity of the turbulence is greatest in the tangential direction.

Recently, large-scale vortical instabilities have also been obtained by Serre *et al.* [90] in a relatively high cavity ($L = 2.33$). In order to explore the very wide range of conditions to be considered, both in configurational and Reynolds number space, complementary experimental studies has been carried out (Czarny *et al.* [91]). In a recent paper, Owen [92] has drawn attention to difficulties in predicting the flow in certain rotor-stator configurations using the assumption of axisymmetry, and speculated that the cause might be related to the formation of large-scale vortical instabilities, as already observed by Abrahamson *et al.* [93] within corotating disks, for both laminar and turbulent regimes. A DNS of Serre *et al.* [90] showed that these structures precess at a rate intermediate between the rotation rates of the two disks, and are only located in the non-viscous geostrophic core that explains why they are increasingly likely to occur as the cavity height relative to the radius is increased. The fact that these structures only occur in the core, could be related to the inertial waves noted by Jacques *et al.* [88] in their two-dimensional DNS at $Re = 10^6$. Flow visualizations (Figure 28) bring out clearly the large structures with an azimuthal periodicity m, that strongly depends on the rotation rate: m decreasing from 7 to 2, from $Re = 58000$ to $Re = 174000$. This behavior is coherent with DNS results showing a structure with $m = 9$ at $Re = 45000$. Such a simulation currently lies outside the scope of DNS, but LES and even time-dependent RANS explorations may hope to capture much of the

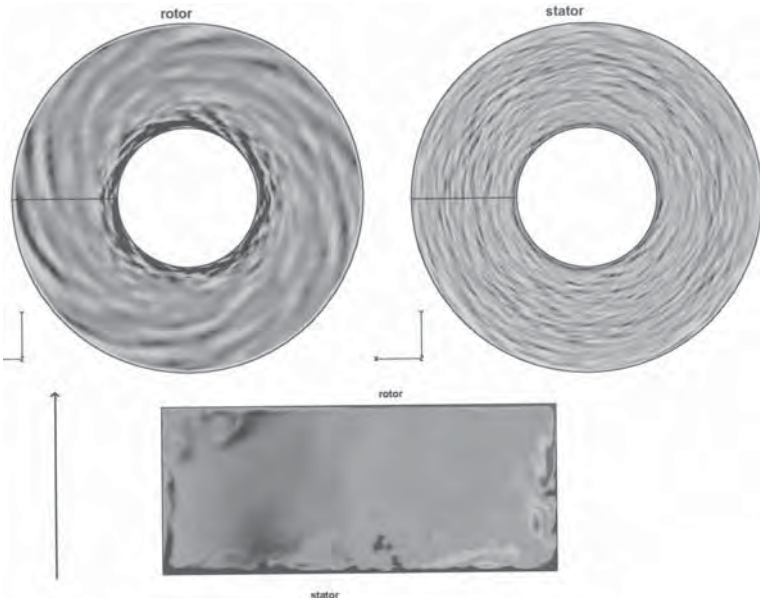

Figure 27: Isosurface of instantaneous tangential velocity in rotor and stator boundary layers and in the meridianal plane at $Re_R = 10^5$.

experimentally observed structures.

For engineering applications, the computations of the (steady) Reynolds-averaged Navier-Stokes equations with various models of turbulence remains the only practicable approach to study turbulent rotor-stator flows in industrial conditions as well as the associated heat or mass transfer. Most works examine the turbulence-modelling problems associated with the numerical computation of axisymmetric flows. These flows typically involve rotating boundary layers, impingement and recirculating flow regions and would thus seem to be very challenging for turbulence modelling. Indeed, the turbulence model must be able to resolve the low Reynolds number regions not only near the disks but also in the core of the flow. Moreover, the model ought to predict the location of transition from the laminar to the turbulent regime, even though the transition process is bounded by instabilities, and so cannot be completely represented by a steady flow model.

There are various turbulence models available and these fall into two categories: those based on an effective eddy viscosity (the mixing-length model: see, for example, Koosinlin *et al.* [95], Chew [96]; the low-Reynolds number $k - \epsilon$ model: see, for example, Jones and Launder [97]; Morse [98]) and those employing the Reynolds stress equations (Launder *et al.* [99]; Elena and Schiestel [100]). The latter are generally held to be more accurate, but are more costly in CPU times for practical applications, even if numerical stability problems are overcome.

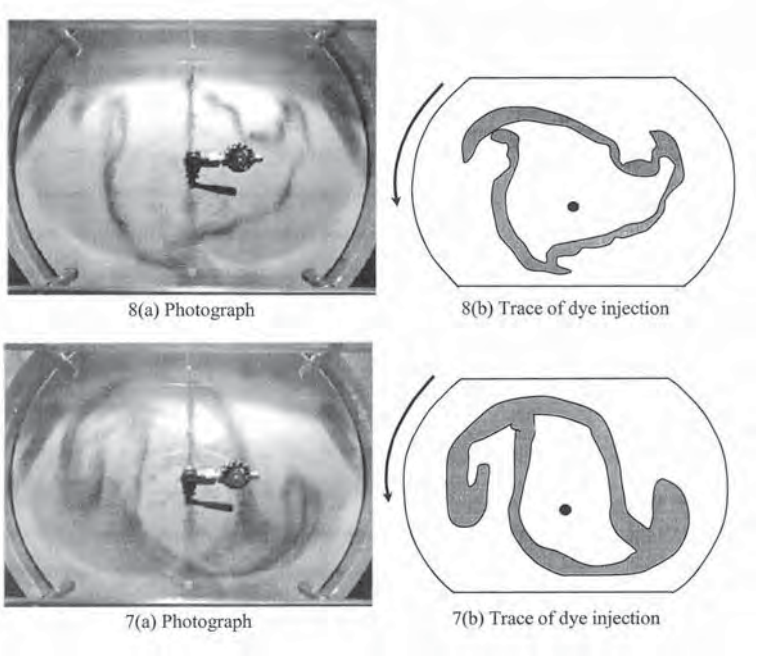

Figure 28: Flow visualizations and schemes of $m = 3$ and $m = 2$ structures (From Czarny *et al.* [91]).

The development of improved models has been an area of extensive research over the last few years. Extensive studies of turbulence models involving an eddy-viscosity approximation in such configurations have been conducted at UMIST. A review of most studies up to 1995 is available in Iacovides and Launder [50].

One of the most important failures of eddy-viscosity models in predicting this type of flow is an overestimate of the extent of the relaminarized zone on the inner part of the rotating disk [101], leading to erroneous Ekman layer predictions and rotation rates in the central core. Iacovides & Theofanoupolos [101] have adopted a zonal modelling with an algebraic stress model in the core of the flow matched to different mixing-length models near the wall. These authors have shown the importance of the near-wall modelling in these flows because the mean-flow driving force results from the interaction between the rotation induced centrifugal forces and the viscosity-driven boundary region.

Other studies of rotor-stator flows and other flows with rotation (Hanjalic and Launder [102]; Launder and Tselepidakis [103]; Randriamampianina *et al.* [64]) have shown that second-moment closures provided a more appropriate level of modelling to predict such complex flows. Up to now, the most extensive comparisons of models have been performed by Elena [94], Elena and Schiestel [104, 100] by comparing different numerical results with the experiments of Itoh *et al.* [62] and Cheah *et al.* [83]. They compared the $k - \epsilon$ model of Launder and Sharma

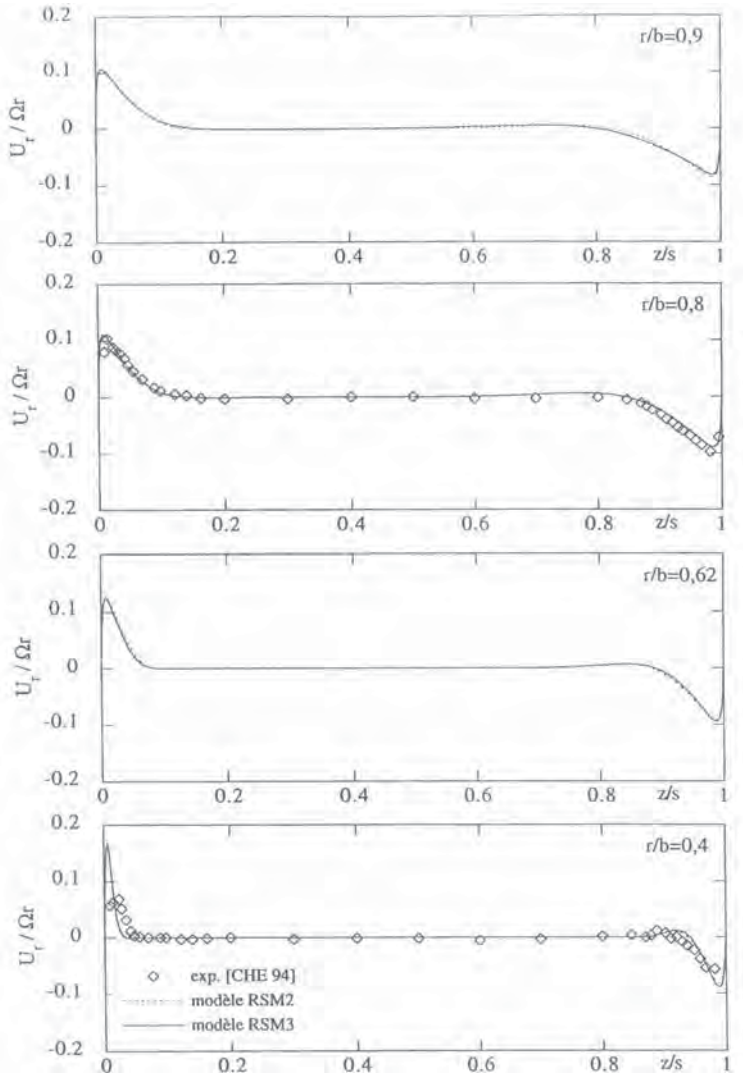

Figure 29: Comparison between experimental results of Cheah *et al.* [83] and numerical results of Elena [94] using two types of Reynolds-stress modelling. Axial profiles of the radial mean velocity at four different radial positions. Rotor-stator cavity, $\Gamma = 7.87$, $Re = 1.6 \times 10^6$ (from Elena [94]).

[105] with the an ASM (algebraic stress model) linked near the wall to the Launder and Sharma [105] model and with the RSM (Reynolds-stress model) of Launder *et al.* [99] with wall echo terms of Gibson and Launder [106]. Elena and Schiestel also tested a more recent RSM by Craft *et al.* [107] (documented in more

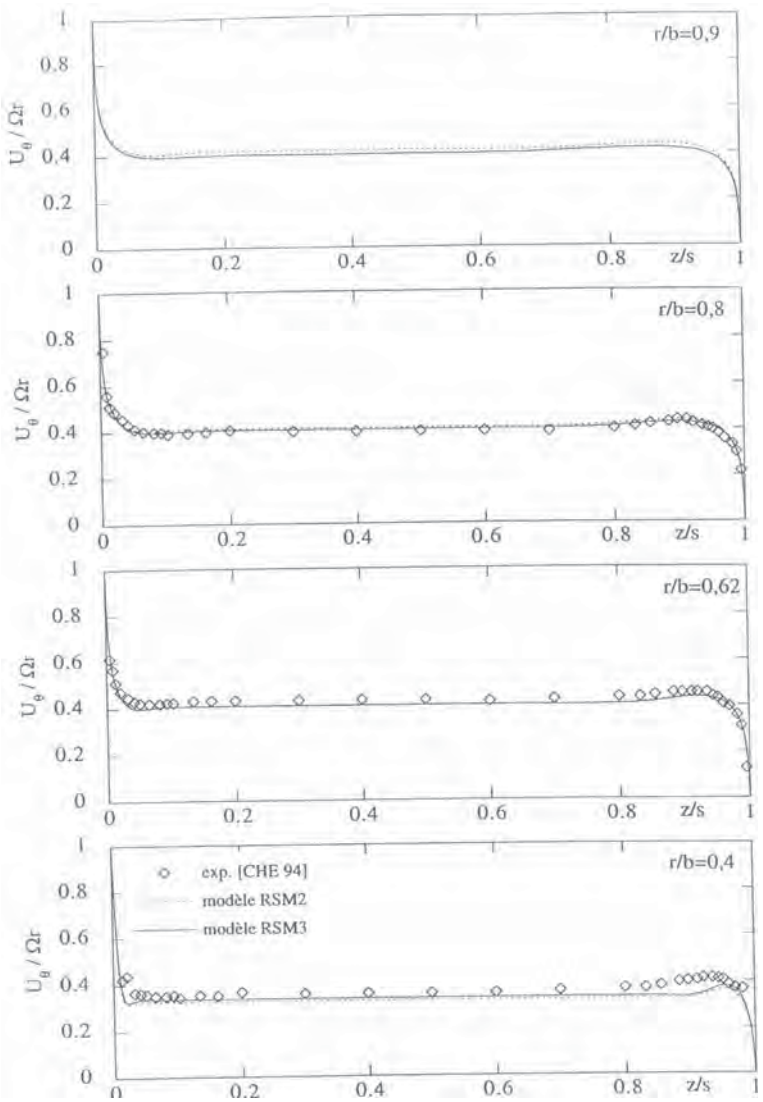

Figure 30: Comparison between experimental results of Cheah *et al.* [83] and numerical results of Elena [94] using two types of Reynolds-stress modelling. Axial profiles of the azimuthal mean velocity at four different radial positions. Rotor-stator cavity, $\Gamma = 7.87$, $Re = 1.6 \times 10^6$ (from Elena [94]).

accessible form in Launder and Li [108] or Craft and Launder [109]) and an elaboration of it that they devised. These latter models are both designed to satisfy the two-component limit (TCL) to which turbulence reduces as one approaches a rigid

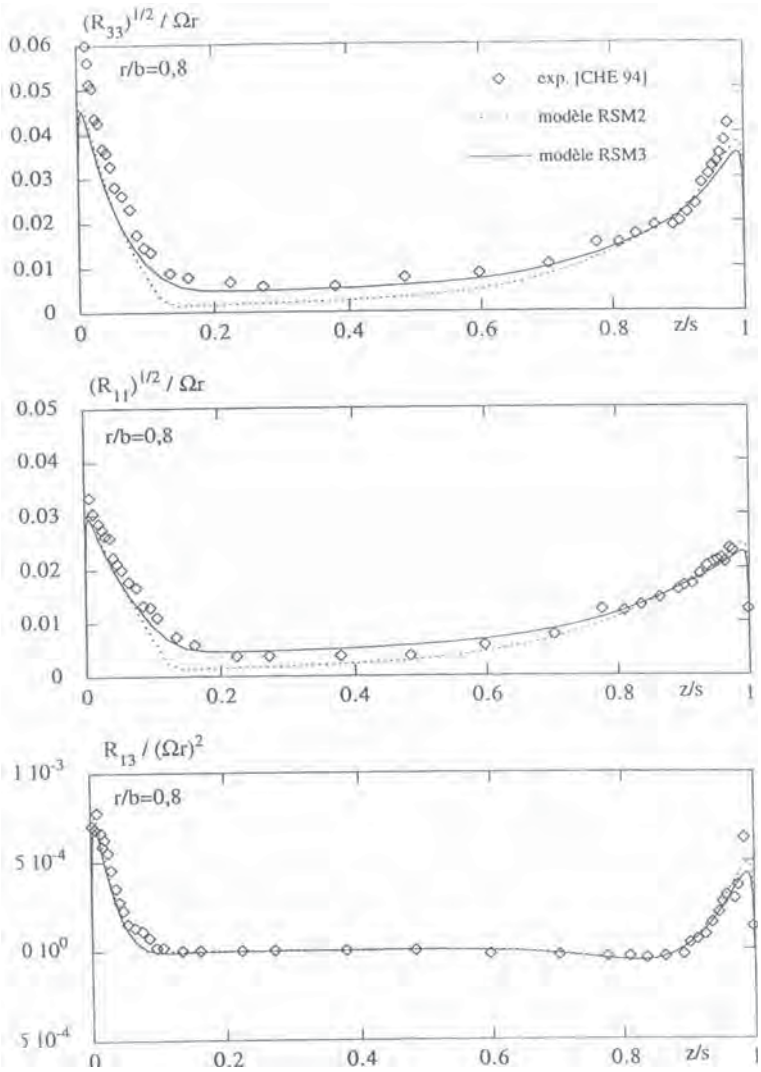

Figure 31: Comparison between experimental results of Cheah *et al.* [83] and numerical results of Elena [94] using two types of Reynolds stress modelling. Axial profiles of the Reynolds-stresses at $r/R_1 = 0.8$. Rotor-stator cavity, $\Gamma = 7.87$, $Re = 1.6 \times 10^6$ (from Elena [94]).

surface. As already mentioned, the results given by the commonly used $k-\epsilon$ model give a too laminar solution which failed completely to mimic k. Second-moment closures (RSM) especially the TCL schemes provide a more accurate description of both the mean flow and the turbulence stress field and a correct distribution of laminar and turbulent regions. Examples of the latter models applied to a test

flow from Cheah *et al.* [83] are reproduced in Figures 29and 30. Of course, it is unlikely that any second-moment closure would be able to reproduce the flow behavior when there are large-scale vortices present such as those shown in Figure 28. However, it would be interesting to explore whether a time-dependent solution of the Reynolds equations might be equal to the task.

Appendix: Numerical approaches in rotating-flow investigations

In this section we present general features of some numerical methods generally used in the investigation of rotating flows in cavities. As there exists an extensive literature on the topic, we shall not attempt to present an exhaustive technical review but will rather focus on general ideas that we believe to be important from our proper experience in the use of these methods in such problems. A general technical review of numerical methods for the Navier-Stokes equations can be found in Ferziger and Peric [110], Peyret and Taylor [111] and more specifically for finite elements and spectral methods in Girault and Raviart [112] and Peyret [113], respectively. As has been noted above, today, computations complement experimental and theoretical approaches in the investigation of rotating flows, providing detailed and comprehensive information as much on the transitional and pre-transitional flow regime as turbulent flow. In particular, the very thin boundary layers close to the walls are very hard to measure without disturbing the flow. High-order numerical methods allow the investigation of small-scale structures located very close to the walls without introducing any uncontrolled perturbation. Moreover, it offers a means of testing theoretical models such as solving the linear Navier-Stokes equations in a stability analysis.

Depending on the best compromise between solution accuracy and computer resources, different approaches exist for obtaining physical solutions to the incompressible Navier-Stokes equations, for a given set of boundary and initial conditions [110].

In direct numerical simulation (DNS), the Navier-Stokes equations are solved to determine quantities (V, p for example) for one realization of the flow, all length-scales and timescales are resolved. This approach is unrivalled in accuracy and level of description provided. However, it is important to appreciate that its cost is high (increases approximately as Re^3), and is limited due to computer performance and cost to flows of low-to-moderate Reynolds numbers corresponding to transition and weakly turbulent regimes. This method also allows the computation of statistical quantities that can be compared to experimental data to validate the results. It also allows one to compute quantities that are difficult or impossible to measure in experiments and that are useful for assessing models, for example the pressure-strain correlation that appears in the Reynolds-stress transport equations.

At high Reynolds numbers, the Navier-Stokes equations can only be solved at present for some mean quantities (the Reynolds-averaged Navier-Stokes equations). On averaging, the non-linearity gives rise to terms (Reynolds stresses) that appear as new unknowns and which have to be approximated with a turbulence model, either via a turbulent-viscosity hypothesis (which may be linear or

non-linear) or more directly from modelled Reynolds-stress (and possibly higher moment) transport equations. Large eddy simulation can be considered as an intermediate approach in which the equations are solved for "filtered" quantities representative of the large-scale turbulent motions. The equations solved include a model for the influence of the smaller-scale motions that are not directly represented. To our knowledge there is no work at the moment using this approach devoted to *confined* rotating flows (see Wu and Squires [78] for the case of a single disk). Indeed, LES remains problematic in near-wall flows, and continues to be very costly, typically two orders of magnitude higher than RANS, and places considerably more stringent constraints than RANS on numerical accuracy and grid quality [114]. While LES will increasingly be used in practical applications where accuracy of simulation has a vital (and expensive) effect on performance of the industrial hardware, it is unlikely to replace RANS, especially in near-wall flows.

The configurations considered in this chapter are simple geometries in order to investigate complex physics within controlled flows. The most important requirements placed on numerical methods for DNS arise from the need to produce an accurate realization of the flow, while for RANS approaches they arise from the robustness of the numerical method in order to overcome the impediments to convergence arising from the greater stiffness. In the $k - \varepsilon$ model for example, two new partial differential equations need to be solved that are much stiffer than the laminar equations, due to the fact that the time-scales associated with the turbulence are much shorter than those connected with the mean flow. The stiffness is the reason why the mean flow and turbulence equations are treated separately. Too large a time step (or its equivalent in an iterative method) can lead to negative values of either k or ε and numerical instability unless traps to prevent these physically unattainable levels are built into the code. It is, in any event, necessary to use under-relaxation techniques in the iterative method for these quantities. Moreover, in RANS approaches the more widely employed numerical methods are based on finite-volume ([50, 104, 100]) and finite-difference ([88]) discretization techniques. The numerical difficulties encountered when solving turbulence closure problems by finite-difference schemes center principally on the difference approximations used for the inertia term and whether the viscous terms for the unsteady case are implicitly or explicitly introduced. As mentioned in Peyret and Taylor [111], the problem basically is that to maintain stability at the high Reynolds numbers explicit central-difference schemes require a very small grid size. As a result, there has been a tendency to introduce one-sided differences for the spatial derivatives in the convective terms. This is exactly equivalent to adding an artificial viscosity to damp oscillations and is equivalent to another closure model.

For most cases, the finite-volume approach has been the preferred numerical strategy because it is mass conservative on each control volume. Consequently, it always provides physical solutions even on relatively coarse grids that allow moderate cost computations to be made even at high Reynolds numbers. Moreover, using a different stabilization approach one can handle equations with complex and non-linear sources such as those found in RANS approaches.

Moreover, we would remark that most other numerical difficulties with turbulence-closure calculations arise from the inadequacy of the model and not the numerics. For example in a two-equation (k, ε) model, the terms with ε/k can be singular in poorly modelled regions of flow and unless traps are explicitly built into the computation divergence will result. Even with traps, however, they will not assure accurate prediction.

In DNS, the equations contain a wide range of length- and time-scales particularly when the Reynolds numbers is high. The requirement for accuracy makes the use of spectral methods common in DNS. The relatively low accuracy of discrete numerical methods used in finite-difference or finite-element schemes can be considered as an obstacle to the representation of complex flows with a very fine structure such as encountered in rotating flows. Nevertheless, many studies use these techniques ([88, 85]) for their relativity simplicity and efficiency on regular grids in particular with the use of fast direct solvers based upon a partial diagonalization technique. For transition and weakly turbulent regimes studied in simple geometries, pseudo-spectral methods are the preferred numerical approach because of their superior accuracy [113]. Indeed, one of the main properties of the Fourier series is its fast rate of convergence which is exponential for infinitely differentiable functions. In the case of non-periodic problems, Chebyshev polynomials can be used as basis functions possessing some of the properties of the Fourier series (rate of convergence, possibility of using FFT algorithm). Moreover, the increasing power of computers and the efficiency of the FFT algorithm for the calculations of the series are fundamental to a fast calculation of the nonlinear terms through the pseudospectral technique and makes this method very efficient. As noted by Peyret and Taylor [111] this method can reduce computation times by more than an order of magnitude over finite-difference techniques for two- and three-dimensional problems, the reason being that these types of expansion need fewer grid points to obtain the same resolution as a second-order finite-difference method [111]. Moreover, the use of the Chebyshev collocation approximation is readily adapted to concentrating grid points close to the thin layers bordering the domain where the smallest-size structures of the flow are located. All these characteristics constitute an obvious advantage over finite-difference or finite-volume methods in the numerical investigation of these types of problems.

We will not give details about time discretization because there is a too large number of techniques used in the literature. We simply note that, because an accurate time history is required, the temporal discretization technique has to ensure a compromise between a small time step required for accuracy and a large time step required to advance in time sufficiently quickly. Moreover, the presence of walls and the use of a very fine grid in the direction normal to the wall means that numerical instabilities may arise from the viscous terms involving derivatives normal to the wall. These are often treated implicitly.

References

[1] Lilly, D.K., On the instability of Ekman boundary layer flow. *J Atmos Sci*, **23**, pp. 481–494, 1966.

[2] Lingwood, R.J., Absolute instability of the boundary layer on a rotating disk. *J Fluid Mech*, **299**, pp. 17–33, 1995.

[3] Lingwood, R.J., An experimental study of absolute instability of the rotating-disk boundary layer flow. *J Fluid Mech*, **314**, pp. 373–405, 1996.

[4] Lingwood, R.J., Absolute instability of the Ekman layer and related rotating flows. *J Fluid Mech*, **331**, pp. 405–428, 1997.

[5] Faller, A.J., Instability and transition of disturbed flow over a rotating disk. *J Fluid Mech*, **230**, pp. 245–269, 1991.

[6] Davies, C. & Carpenter, P.W., Global behaviour corresponding to the absolute instability of the rotating-disc boundary layer. *J Fluid Mech*, **486**, pp. 287–329, 2003.

[7] Reed, H.L. & Saric, W.S., Stability and transition of three-dimensional boundary layers. *Ann Rev Fluid Mech*, **35**, pp. 413–440, 2003.

[8] Pier, B., Finite-amplitude crossflow vortices, secondary instability and transition in the rotating-disk boundary layer. *J Fluid Mech*, **487**, pp. 315–343, 2003.

[9] Cambon, C. & Jacquin, L., Spectral approach to non-isotropic turbulence subjected to rotation. *J Fluid Mech*, **202**, pp. 295–317, 1989.

[10] Nagano, Y., Tagawa, M. & Tsuji, T., Effects of adverse pressure gradients on means flows and turbulence statistics in a boundary layer. *Proceedings of TSF8; Technical Univ of Munich*, 1991.

[11] Greenspan, H., Numerical studies of flow between rotating coaxial disks. *J Inst Maths Applics*, **9**, pp. 370–377, 1972.

[12] Schlichting, H., *Boundary Layer Theory*. McGraw Hill: New York, 7th edition, 1979.

[13] Greenspan, H., *The Theory of Rotating Fluids*. Cambridge University Press: Cambridge, 1969.

[14] Reed, H.L. & Saric, W.S., Stability of three-dimensional boundary layers. *Ann Rev Fluid Mech*, **22**, pp. 235–284, 1989.

[15] Faller, A.J. & Kaylor, R.E., A numerical study of the instability of the laminar Ekman boundary layer note on the class of solutions of Navier-Stokes equations representing steady rotationally-symmetric flows. *J Atm Sci*, **23**, pp. 466–480, 1966.

[16] Faller, A.J. & Kaylor, A.J., Instability of Ekman spiral with application to planetary boundary layer. *Phys Fluids*, **19(9)**, p. 212, 1967.

[17] Briggs, R., *Electron-Stream Interaction with Plasmas*. MIT Press: Berlin and New York, 1964.

[18] Huerre, P. & Monkewitz, P., Local and global instability in spatially developing flows. *Annu Rev Fluid Mech*, **22**, pp. 473–500, 1990.

[19] Huerre, P., *Open shear flow instabilities*. Perspectives in Fluid Dynamics, G. K. Batchelor, H. K. Moffat and M. G. Worster, Cambridge University

Press: Cambridge, pp. 159–228, 2000.
[20] Stewart, R.H., *Introduction to Physical Oceanography*. http://oceanworld.tamu.edu/resources/ocng_textbook/contents.html: Texas A&M University, 1998.
[21] Pedlosky, J., *Geophysical Fluid Dynamics*. Springer-Verlag: Berlin, 2nd edition, 1984.
[22] Tritton, D.J., *Physical Fluid Dynamics*. Clarendon Press: Oxford, 2nd edition, 1988.
[23] Itoh, M., On the instability of flow between coaxial rotating disks. *ASME, Boundary Layer Stability and Transition to Turbulence*, **114**, pp. 83–89, 1991.
[24] Serre, E., Tuliszka-Sznitko, E. & Bontoux, P., Coupled numerical and theoretical study of the flow transition between a rotating a stationary disk. *Phys Fluids*, 2004, in print.
[25] Faller, A.J., An experimental study of the instability of the laminar Ekman boundary layer. *J Fluid Mech*, **15**, pp. 560–576, 1963.
[26] Tatro, P.R. & Mollo-Christensen, E., Experiments on Ekman-layer instability. *J Fluid Mech*, **28**, pp. 531–544, 1967.
[27] Cerasoli, C.J., Free shear layer instability due to probes in rotating source-sink flows. *J Fluid Mech*, **72(3)**, pp. 559–586, 1975.
[28] Owen, J.M., Pincombe, J.R. & Rogers, R., Source-sink flow in side a rotating cylindrical cavity. *J Fluid Mech*, **155**, pp. 233–265, 1985.
[29] Haeusser, T.M. & Leibovich, S., Pattern formation in the marginally unstable Ekman layer. *J Fluid Mech*, **479**, pp. 125–144, 2003.
[30] Wilkinson, S.P. & Malik, M.R., Stability experiments in the flow over a rotating disk. *AIAA Journal*, **23(4)**, pp. 588–595, 1985.
[31] Gregory, N., Stuart, J. & Walker, W., On the stability of three-dimensional boundary layers with application to the the flow due to a rotating disk. *Phil Trans R Soc London*, **248**, pp. 155–199, 1955.
[32] Jarre, S., Le Gal, P. & Chauve, M.P., Experimental study of rotating disk instability. I. Natural flow. *Phys of Fluids*, **8(2)**, pp. 496–508, 1996.
[33] Mack, L., The wave pattern produced by point source on a rotating disk. *AIAA*, **85-0490**, 1985.
[34] Pikhtov, S.V. & Smirnov, E.M., Boundary layer stability on a rotating disk with corotation of the surrounding fluid. *J Fluid Dyn*, **27(3)**, pp. 657–663, 1992.
[35] Savas, O., Stability of Bödewadt flow. *J Fluid Mech*, **183**, pp. 77–94, 1987.
[36] Lopez, J., Flow between a stationary and a rotating disk shrouded by a corotating cylinder. *Phys of Fluids*, **8**, pp. 2605–2613, 1996.
[37] Batchelor, G., Note on the class of solutions of the Navier-Stokes equations presenting steady rotationally-symmetric flow. *QJ Mech Appl Maths*, **4**, pp. 29–41, 1951.
[38] Stewartson, K., On the flow between two rotating coaxial disks. *Proc Camb Phil Soc*, **49**, pp. 333–341, 1953.
[39] Zandbergen, P. & Dijkstra, D., Von Kármán swirling flows. *Ann Rev Fluid*

Mech, **19**, pp. 465–491, 1987.
[40] Mellor, G., Chapple, P. & Stokes, V., On the flow between a rotating and a stationary disk. *J Fluid Mech*, **31**, pp. 95–112, 1968.
[41] Pearson, C.E., Numerical solutions for the time-dependent viscous flow between two rotating coaxial disks. *J Fluid Mech*, **21(4)**, pp. 623–633, 1965.
[42] Brady, J. & Durlofsky, L., On rotating disk flow. *J Fluid Mech*, **175**, pp. 363–394, 1987.
[43] Dijkstra, D. & Heijst, G., The flow between two finite rotating disks enclosed by a cylinder. *J Fluid Mech*, **128**, pp. 123–154, 1983.
[44] San'kov, P. & Smirnov, E., Bifurcation and transition to turbulence in the gap between rotating and stationary parallel disks. *Int J Fluid Dyn*, **19(5)**, pp. 695–705, 1984.
[45] Owen, J.M. & Rogers, R., *Heat Transfer in Rotating Disk Systems, Vol. 1: Rotor-Stator Systems*. Editor W. D. Morris (Wiley, Taunton, Somerset, England), 1989.
[46] Owen, J.M. & Rogers, R.H., *Heat Transfer in Rotating Disk Systems, Vol. 2: Rotating Cavities*. Editor W. D. Morris (Wiley, Taunton, Somerset, England), 1995.
[47] Gauthier, G., Gondret, P. & Rabaud, M., Axisymmetric propagating vortices in the flow between a rotating and a stationary disk enclosed by a cylinder. *J Fluid Mech*, **386**, pp. 105–126, 1999.
[48] Schouveiler, L., Le Gal, P. & Chauve, M.P., Instabilities of flow between a rotating and a stationary disk. *J Fluid Mech*, **443**, pp. 329–350, 2001.
[49] Serre, E., Crespo del Arco, E. & Bontoux, P., Annular and spiral patterns between a rotating and a stationary disk. *J Fluid Mech*, **434**, pp. 65–100, 2001.
[50] Iacovides, H. & Launder, B., Computational fluid dynamics applied to internal gas-turbine blade cooling: a review. *Int J Heat Fluid Flow*, **16**, pp. 454–470, 1995.
[51] Crespo del Arco, E., Maubert, P., Randriamampianina, A. & Bontoux, P., Spatio-temporal behaviour in a rotating annulus with a source-sink flow. *J Fluid Mech*, **32**, pp. 1–27, 1996.
[52] Schouveiler, L., Le Gal, P., Chauve, M.P. & Takeda, Y., *Experimental Study of the Stability of the Flow between a Rotating and a Stationary Disk*. Advances in Turbulence VI, Editors: Gavrilakis S, Machiels L, Monkewitz PA Fluid Mechanics and its Applications, 36, pp. 385–388, 1996.
[53] Escudier, M., Observations of the flow produced in a cylindrical container by a rotating endwall. *Exps Fluids*, **2**, pp. 1–21, 1984.
[54] Gelfgat, Y., Bar-Joseph, P. & Solan, A., Three-dimensional instability of axisymmetric flow in a rotating lid-cylinder enclosure. *J Fluid Mech*, **438**, pp. 363–377, 2001.
[55] Marques, F. & Lopez, J., Precessing vortex breakdown mode in an enclosed cylinder flow. *Phys Fluids*, **13**, pp. 1679–1682, 2001.
[56] Blackburn, H. & Lopez, J., Modulated rotating waves in an enclosed swirling flow. *J Fluid Mech*, **465**, pp. 33–58, 2002.

[57] Serre, E. & Bontoux, P., Vortex breakdown in a three-dimensional swirling flow. *J Fluid Mechanics*, **459**, pp. 347–370, 2002.
[58] Spohn, A., Mory, M. & Hopfinger, E., Experiments on vortex breakdown in a confined flow generated by a rotating disk. *J Fluid Mech*, **370**, pp. 73–99, 1998.
[59] Sotiropoulos, F. & Ventikos, Y., Transition from bubble-type vortex breakdown to columnar vortex in confined swirling flow. *Intl J Heat Fluid Flow*, **19**, pp. 446–458, 1998.
[60] Sotiropoulos, F. & Ventikos, Y., The three-dimensional structure of confined swirling flows with vortex breakdown. *J Fluid Mech*, **426**, pp. 155–175, 2001.
[61] Cros, A. & Le Gal, P., Instabilities of the flow between a rotating and a stationary disk. *Phys Fluids*, **14(11)**, pp. 3755–3765, 2002.
[62] Itoh, M., Yamada, Y., Imao, S. & Gonda, M., Experiments on turbulent flow due to an enclosed rotating disc. *Exptl Thermal Fluid Sci*, **5**, pp. 359–368, 1992.
[63] Sirivat, A., Stability experiment of flow between a stationary and a rotating disk. *Phys Fluids*, **3(11)**, pp. 2664–2671, 1991.
[64] Randriamampianina, A., Elena, L., Fontaine, J. & Schiestel, R., Numerical prediction of laminar, transitional and turbulent flows in shrouded rotor-stator systems. *Phys of Fluids*, **9(6)**, pp. 1696–1713, 1997.
[65] Fernandez-Feria, R., Axisymmetric instabilities of Bödewadt flow. *Phys Fluids*, **12(7)**, pp. 1730–1739, 2000.
[66] Lopez, J. & Weidman, P., Stability of stationary endwall boundary layers during spin-down. *J Fluid Mech*, **326**, pp. 373–398, 1996.
[67] Schouveiler, L., Le Gal, P. & Chauve, M.P., Stability of a roll travelling system in a rotating disk flow. *Phys Fluids*, **10(1)**, pp. 2695–2697, 1998.
[68] Cousin-Rittemard, N., Daube, O. & Le Quéré, P., Sur la nature de la premiére bifurcation des écoulements interdisques. *CR Acad Sci Paris*, **326**, pp. 359–366, 1998.
[69] Savas, O., Circular waves on a stationary disk in rotating flow. *Phys Fluids*, **26(12)**, pp. 3445–3448, 1983.
[70] Daube, O. & Le Quéré, P., Numerical investigation of the first bifurcation for the flow in a rotor-stator cavity of radial aspect ratio 10. *Computers and Fluids*, **31**, pp. 481–501, 2002.
[71] Tuliska-Sznitko, E., Serre, E. & Bontoux, P., On the nature of the boundary layer instability in a closed rotor-stator cavity. *C R Acad Sci*, **329(Série IIb)**, pp. 91–99, 2002.
[72] Schouveiler, L., Sur les instabilités de l'écoulement entre un disque fixe et un disque en rotation. *PhD Thesis, Université Aix-Marseille*, 1998.
[73] Arons, A.B., Ingersoll, A.P. & T. Green, I., Experimentally observed instability of a laminar Ekman flow in a rotating basin. *Tellus*, **13**, pp. 31–39, 1961.
[74] Hide, R., On source-sink flows stratified in a rotating annulus. *J Fluid Mech*, **32**, pp. 737–764, 1968.

[75] Serre, E., Hugues, S., Crespo del Arco, E., Randriamampianina, A. & Bontoux, P., Axisymmetric and three-dimensional instabilities in an Ekman boundary layer flow. *Intl J Heat Fluid Flow*, **22**, pp. 82–93, 2001.
[76] Caldwell, D. & Van Atta, C.W., Characteristics of Ekman boundary layer instabilities. *J Fluid Mech*, **44**, pp. 79–95, 1970.
[77] Littell, H. & Eaton, J., Turbulence characteristics of the boundary layer on a rotating disk. *J Fluid Mech*, **266**, pp. 175–207, 1994.
[78] Wu, X. & Squires, K., Prediction and investigation of the turbulent flow over a rotating disk. *J Fluid Mech*, **418**, pp. 231–264, 2000.
[79] Schmid, P. & Henningson, D., *Stability and Transition in Shear Flows*. Springer: Berlin, 2000.
[80] Schmid, P. & Henningson, D., Stability and transition of three-dimensional boundary layers. *Ann Rev Fluid Mech*, **35**, pp. 413–440, 2003.
[81] Saric, W.S., Reed, H.L. & White, E.B., Stability and transition of three-dimensional boundary layers. *Ann Rev Fluid Mech*, **35**, pp. 413–440, 2003.
[82] Daily, J. & Nece, R., Chamber dimension effects on induced flow and frictionnal resistence of enclosed rotating discs. *J Basic Eng*, **82**, p. 217, 1960.
[83] Cheah, S.C., Iacovides, H., Jackson, D. & Launder, B.E., Experimental investigation of enclosed rotor-stator disc flows. *J Exp Therm Fluid Sci*, **9**, pp. 445–468, 1994.
[84] Pao, H.P., A numerical computation of a confined rotating disc. *Trans ASME J Appl Mech*, **92**, pp. 480–, 1970.
[85] Lygren, M. & Andersson, H., Turbulent flow between a rotating and a stationary disk. *J Fluid Mech*, **426**, pp. 297–326, 2001.
[86] Jeong, J., Hussain, F., Schoppa, W. & Kim, J., Coherent structures near the wall in a turbulent channel flow. *J Fluid Mech*, **332**, pp. 185–214, 1997.
[87] Jeong, J. & Hussain, F., On the identification of a vortex. *J Fluid Mech*, **285**, pp. 69–94, 1995.
[88] Jacques, R., Daube, O. & Le Quéré, P., Axisymmetric numerical simulations of turbulent flow in rotor-stator enclosures. *Int J of Heat and Fluid Flows*, **23**, pp. 381–397, 2002.
[89] Serre, E., Bontoux, P. & Launder, B., Direct numerical simulation of transitional turbulent flow in an enclosed rotor-stator cavity. *Int J Flow, Turbulence and Combustion*, **69**, pp. 35–50, 2002.
[90] Serre, E., Czarny, O., Iacovides, H., Bontoux, P. & Launder, B., *Precessing Vortex Structures within Rotor-Stator Disk: DNS Visualization Studies*. CIMNE Barcelona: Barcelona, pp. 421–424, 2002.
[91] Czarny, O., Iacovides, H. & Launder, B., Precessing vortex structures in turbulent flow within rotor-stator discs cavities. *J Flow, Turbulence and Combustion*, **69(1)**, pp. 51–61, 2002.
[92] Owen, J.M., Flow and heat transfer in rotating disc systems. *Turbulence Heat and Mass Transfer*, pp. 33–58, 2000.
[93] Abrahamson, S.M., Eaton, J. & Koga, D., The flow between shrouded corotating disks. *Phys Fluids A*, **1**, pp. 241–251, 1991.

[94] Elena, L., Modelisation de la turbulence inhomogéne en présence de rotation. *PhD Thesis, Université Aix-Marseille*, 1996.
[95] Koosinlin, M., Launder, B.E. & Sharma, B.I., Prediction of momentum heat and mass transfer in swirling turbulent boundary layers. *ASME J Heat Mass Transfer*, pp. 204–209, 1974.
[96] Chew, J., Prediction of flow in a rotating cavity with radial outflow using a mixing length turbulence model. *TSGO193, Rolls Royce report*, 1985.
[97] Jones, W.P. & Launder, B.E., The calculation of low-Reynolds number phenomena with a two equation model of turbulence. *Int J Heat Mass Transfer*, **16**, pp. 1119–, 1973.
[98] Morse, A., Numerical prediction of turbulent flow in rotating cavities. *ASME, J Turbomachinary*, **110**, pp. 202–212, 1988.
[99] Launder, B.E., Reece, G.J. & Rodi, W., Progress in the developpement of a Reynolds stress closure. *J Fluid Mech*, **63(3)**, pp. 537–566, 1975.
[100] Elena, L. & Schiestel, R., Turbulence modeling of rotating confined flow. *Int J Heat Fluid Flow*, **17**, pp. 283–289, 1996.
[101] Iacovides, H. & Theofanoupolos, I., Turbulence modelling of axisymmetric flow inside rotating cavities. *Int J Heat Fluid Flow*, **12**, pp. 2–, 1991.
[102] Hanjalic, K. & Launder, B., Contribution towards a Reynolds stress closure for low-Reynolds number turbulence. *J Fluid Mech*, **74**, p. 593, 1976.
[103] Launder, B.E. & Tselepidakis, D., Application of a new second moment closure to turbulent channel flow rotating in orthogonal mode. *Int J Heat Fluid Flow*, **15**, pp. 2–, 1994.
[104] Elena, L. & Schiestel, R., Turbulence modeling of confined flow in rotating disc system. *AIAA*, **33**, pp. 812–821, 1994.
[105] Launder, B.E. & Sharma, B., Application of the enrgy dissipation model; of turbulence to the calculation of a flow near a spinning disk. *Letters in Heat and Mass Transfer*, **1**, pp. 131–138, 1974.
[106] Gibson, M. & Launder, B., Ground effects on pressure fluctuations in ythe atmospheric boundary layer. *J Fluid Mech*, **86**, pp. 491–511, 1978.
[107] Craft, T., Fu, S., Launder, B. & Tselipidakis, D., Developments in modelling the turbulent second-moment pressure correlations. *Rep TFD/89/1 Dept Mech Eng'g UMIST*, 1989.
[108] Launder, B.E. & Li, S., On the elimination of wall-topography parameters from second-moment closure. *Phys of Fluids*, **6**, pp. 999–1006, 1994.
[109] Craft, T. & Launder, B., *Closure modelling near the two- component limit (Chapter 3). Closure Strategies for Turbulent and Transitional Flows*. Ed. B. E. Launder & Neil Sandham, Cambridge, 2002.
[110] Ferziger, J. & Peric, M., *Computational Methods for Fluid Dynamics*. Springer-Verlag: Berlin and New York, 2002.
[111] Peyret, R. & Taylor, T., *Computational Methods for Fluid Flow*. Springer-Verlag: Berlin and New York, 1983.
[112] Girault, V. & Raviart, P., *Finite Element Methods for Navier-Stokes Equations*. Springer-Verlag: Berlin and New York, 1986.

[113] Peyret, R., *Spectral methods for incompressible viscous flow*. Springer-Verlag: Berlin and New York, 2002.
[114] Leschziner, M., Modelling separation from curved surfaces with anisotropy-resolving turbulence closures and related supplementary observations on LES. *Proc of Conf on Modelling Fluid Flow (CMFS03) Budapest, Hungary, September 3-6*, 2003.